

**PREPARATION AND CHARACTERIZATION OF ETHYLENE VINYL ACETATE
COPOLYMER/POLY(LACTIC ACID)/SUGARCANE BAGASSE COMPOSITES FOR
WATER PURIFICATION**

by

THOLLWANA ANDRETTA MAKHETHA (B.Sc. Hons.)

2009062932

Submitted in accordance with the requirements for the degree

MASTER OF SCIENCE (M.Sc.)

Department of Chemistry

Faculty of Natural and Agricultural Sciences

at the

UNIVERSITY OF THE FREE STATE (QWAQWA CAMPUS)

SUPERVISOR: MR K. MPITSO

CO-SUPERVISOR: PROF A.S. LUYT

January 2016

DECLARATION

I declare that the thesis hereby submitted by me for the Master of Science degree at the University of the Free State is my own independent work and has not previously been submitted by me at another university/faculty. I furthermore cede copyright of the thesis in favour of the University of the Free State.



Makhetha T.A. (Ms)

DEDICATION

This work is dedicated to the entire family of Makhetha and Nyilika for their love and support. To Maofela Beauty Makhetha (mom), Musuwe Edward Makhetha (father), Nongwenynkomo Roselinah Nyilika (grandmother) whose support and perseverance is gently appreciated and who instilled in me the importance of education at an early age and to Karabo Makhetha (sister).

“Now I believe and I declare my life will never be the same again”

ABSTRACT

Excessive release of heavy metals into the environment due to industrialization and urbanization has posed a great problem to the world. Heavy metal ions do not degrade, therefore they can give bad effect to human body and the environment itself. The purpose of this study was to prepare polymer/natural fibre composites to be used in water purification, specifically to remove lead ions from contaminated water. PLA/EVA blends and PLA/EVA/SCB composites were successfully prepared by melt mixing. The lower viscosity of PLA, the lower interfacial tension between PLA and SCB, and the wetting coefficient of PLA/SCB being larger than 1, all suggested that SCB would preferably be in contact with PLA, despite PLA's relatively high crystallinity. A fairly good dispersion of SCB in the PLA matrix was observed. PLA and EVA were also completely immiscible, with the 50/50 w/w PLA/EVA sample showing a co-continuous morphology and the 70/30 w/w sample showing EVA dispersed as small spheres in the continuous PLA phase. Exposed fibre ends were observed in the composites in some SEM pictures which were believed to add to the efficiency of metal adsorption. The two polymers in the blend seemed to have protected the SCB from thermal degradation, because the mass loss of SCB degradation products was only observed at higher temperatures when incorporated in the blends. Although this behaviour may imply that the prepared composites can be used at temperatures above 200 °C, which is the degradation temperature of pure SCB, it is also possible that the release of the volatile SCB degradation products was delayed as a result of interaction with one or both polymers. The impact properties depended more on the PLA:EVA ratio than on the presence of SCB. The PLA/EVA blends showed two melting peaks at approximately the same temperatures as those of the neat polymers, which confirms the complete immiscibility of PLA and EVA at all investigated compositions.

It was further observed that the water absorption increased with an increase in SCB loading in the composites. The main parameters that influenced lead ion sorption on SCB and PLA/EVA/SCB composites were the initial concentration, contact time, and the pH value. It was observed that more lead was adsorbed than one would expect if the partial coverage of the fibre by the polymer is taken into account, and therefore it may be assumed that some of the lead was trapped inside the cavities in the composites and that the polymers may also have played a role in the metal complexation process, since both polymers have functional groups that could interact with the lead ions. The metal impurities underwent monolayer adsorption.

TABLE OF CONTENTS

	Page
DECLARATION	i
DEDICATION	ii
ABSTRACT	iii
TABLE OF CONTENTS	iv
LIST OF TABLES	vi
LIST OF FIGURES	vii
LIST OF ABBREVIATIONS AND SYMBOLS	ix
CHAPTER 1 (Introduction and literature review)	1
1.1 General introduction	1
1.2 Literature review	4
1.2.1 Natural fibres: Sources and classification	4
1.2.2 Properties of natural fibres	5
1.2.2.1 Structure, physical, and mechanical properties of natural fibres	8
1.2.3 Sugarcane bagasse (SCB)	9
1.2.3.1 Chemical composition of SCB	10
1.2.3.2 Thermal properties of SCB	10
1.2.4 Composite properties	11
1.2.4.1 Modification of polymer/natural fibre composites	11
1.2.4.2 Morphologies of polymer blends/natural fibre composites	12
1.2.4.3 Mechanical properties of polymer blends/natural fibre composites	13
1.2.5 Water absorption of polymer/natural fibre composites	14
1.2.6 Adsorption	14
1.2.6.1 Uses of natural fibres as adsorbents in water treatment	15
1.2.6.2 Adsorption isotherms	16

1.3	Aims and objectives	19
1.4	Outline of the thesis	19
1.5	References	19
CHAPTER 2 (Materials and methods)		34
2.1	Materials	34
2.2	Methods	35
2.2.1	Pre-treatment of sugarcane bagasse	35
2.2.2	Sample preparation	35
2.3	Sample analysis	36
2.4	References	41
CHAPTER 3 (Results and discussion)		43
3.1	Selective dispersion of the SCB in the polymer blends	43
3.2	Morphology	45
3.2.1	Optical microscopy	45
3.2.2	Scanning electron microscopy (SEM)	47
3.2.3	Fourier-transform infrared (FTIR) spectroscopy	49
3.3	Impact strength	51
3.4	Thermal analysis	53
3.4.1	Thermogravimetric analysis (TGA)	53
3.4.2	Differential scanning calorimetry (DSC)	57
3.5	Water absorption	63
3.6	Atomic absorption spectroscopy (AAS)	65
3.7	References	72
CHAPTER 4 (Conclusions)		78
ACKNOWLEDGEMENTS		80
APPENDIX		81

LIST OF TABLES

		Page
Table 2.1	Composition of SCB	34
Table 2.2	Sample compositions used in this study	36
Table 3.1	MFI, density and surface properties of PLA, EVA and SCB	44
Table 3.2	Interfacial tension and wetting coefficient of the investigated materials	45
Table 3.3	Impact properties of all the investigated samples	53
Table 3.4	TGA results for investigated samples	54
Table 3.5	Melting and crystallization temperatures and enthalpies of EVA in the blends and composites	61
Table 3.6	Melting and crystallization temperatures and enthalpies of PLA in the blends and composites	62
Table 3.7	AAS results of all investigated samples at different initial concentrations	66
Table 3.8	AAS results of all investigated samples at different pH level	67
Table 3.9	AAS results of all investigated samples at different contact time	68
Table 3.10	Freundlich isotherm constants for the sorption of lead Pb(II) ions by the different composite samples	70
Table 3.11	Langmuir isotherm constants for the sorption of lead Pb(II) ions by different composite samples	72

LIST OF FIGURES

	Page	
Figure 1.1	Chemical structure of cellulose	6
Figure 1.2	Chemical structure of hemicellulose	7
Figure 1.3	Chemical structure of lignin	7
Figure 1.4	Structure of natural fibre cell	9
Figure 3.1	Optical microscopy pictures of (a) 66.5/28.5/5 w/w PLA/EVA/SCB, (b) 59.5/25.5/15 w/w PLA/EVA/SCB, (c) 56/24/20 w/w PLA/EVA/SCB and (d) 49/21/30 w/w PLA/EVA/SCB	46
Figure 3.2	Optical microscopy images of (a) 80/20 w/w PLA/SCB, and (b) 80/20 w/w EVA/SCB	46
Figure 3.3	SEM images of the fractured surfaces of (a) 50/50 w/w PLA/EVA, (b) 47.5/47.5/5 w/w PLA/EVA/SCB, (c) 42.5/42.5/15 w/w PLA/EVA/SCB, (d) 35/35/30 w/w PLA/EVA/SCB, (e) 70/30 w/w PLA/EVA, (f) 66.5/28.5/5 w/w PLA/EVA/SCB, (g) 59.5/25.5/15 w/w PLA/EVA/SCB, and (h) 49/21/30 w/w PLA/EVA/SCB	48
Figure 3.4	FTIR spectrum of SCB	50
Figure 3.5	FTIR spectra of the PLA/EVA blend and the PLA/EVA/SCB bio-composites	51
Figure 3.6	Impact strengths of the PLA/EVA blends and PLA/EVA/SCB composites at different SCB contents	52
Figure 3.7	(a) TGA and (b) derivative TGA curves of PLA, EVA and SCB	55
Figure 3.8	(a) TGA and (b) derivative TGA curves of 70/30 w/w PLA/EVA and its bio-composites	56
Figure 3.9	DSC second heating curves of the neat PLA, neat EVA, the 50/50 PLA/EVA blend and composites based on its blend	57
Figure 3.10	DSC second heating curves of the neat PLA, neat EVA, the 70/30 PLA/EVA blend and composites based on its blend	59

Figure 3.11	DSC cooling curves of PLA, neat EVA, the 50/50 PLA/EVA blend and composites based on its blend	59
Figure 3.12	DSC cooling curves of PLA, neat EVA, the 70/30 PLA/EVA blend and composites based on its blend	60
Figure 3.13	Water absorption curves and composites based on (a) 50/50 and (b) 70/30 w/w PLA/EVA	64
Figure 3.14	Freundlich plots from which the data in Table 3.7 were obtained	70
Figure 3.15	Langmuir plots from which the data in Table 3.7 were obtained	72

LIST OF ABBREVIATIONS AND SYMBOLS

γ^d	dispersive component of surface energy
γ^p	polar component of surface energy
ω_α	wetting coefficient
AAS	atomic absorption spectroscopy
b	sorption energy
BHT	butylated hydroxy toluene
C_a	adsorbed concentration
C_e	final concentration
C_o	initial concentration
DCP	dicumyl peroxide
ΔH_c	crystallization enthalpy
ΔH_{cc}	cold crystallization enthalpy
ΔH_c^n	normalised cold crystallization enthalpy
ΔH_{cc}^n	normalised crystallization enthalpy
ΔH_m	melting enthalpy
ΔH_m^n	normalised melting enthalpy
ΔH_m°	specific enthalpy of melting
DSC	differential scanning calorimetry
EVA	ethylene vinyl acetate
FTIR	Fourier-transform infrared spectroscopy
γ	surface energy
K_F	adsorption capacity
MFI	melt flow index
n	adsorption intensity
PBSA	polybutylene succinate adipate copolymer
PCL	poly(ϵ -caprolactone)
phr	parts per hundred rubber
PLA	poly(lactic acid)
PLLA	poly(L-lactic acid)
q_e	equilibrium adsorption capacity
q_m	sorption capacity

R^2	significant correlation
R_L	separation factor
rpm	revolutions per minute
SCB	sugarcane bagasse
SEM	scanning electron microscopy
T_{cc}	cold crystallization temperature
T_g	glass transition
TGA	thermogravimetric analysis
T_m	melting temperature
TPS	thermoplastic starch
V	volume
VA	vinyl acetate
w_a	actual mass

CHAPTER 1

Introduction and literature review

1.1 General introduction

Water pollution by heavy metals has received a lot of attention across the world. The metals which contaminate water are produced from liquid waste discharged from a number of industries such as electroplating, textiles, tanneries, oil refineries, mining, and smelters. The most toxic metals, even at lower concentrations, are copper, zinc, lead, chromium, cadmium and nickel. These metals can damage nerves, liver, bones and also interfere with the normal functioning of various metallo-enzymes. They can cause high blood pressure, harmful effect on kidneys, electrolyte imbalance, stomach cramps and allergic skin reaction. Lead ion is a hazardous material that is commonly found in industrial wastewater, thus its removal is of utmost importance. It causes plant and animal death as well as anemia, brain damage, mental deficiency, anorexia, vomiting and malaise in humans [1-5]. Consequently, there is a need to look into new and different methods of removing lead from aqueous medium.

Various methods have been used for the removal of heavy metals from aqueous solution. These methods include membrane filtration [6,7], coagulation and precipitation [8-13], ion-exchange [14,15] and adsorption [16-20]. Only a few of these methods have been accepted due to low cost, efficiency and applicability to a wide variety of pollutants [14]. Membrane filtration is capable of reducing heavy metals at low concentrations. However, the major problem of this method is limited life time before membrane fouling occurs [6,7]. Coagulation and precipitation methods have been widely used for the removal of heavy metals [8-13]. At high pH levels, heavy metals can be precipitated as insoluble hydroxide or sometimes as sulphides. The disposal of the precipitated waste has been the main problem with these methods. Ion-exchange is metal selective, it has a limited pH tolerance, high regeneration and does not present a sludge disposal problem like coagulation and precipitation [14,15]. However, ion-exchange has both high initial capital and maintenance costs [15]. Amongst the mentioned methods, adsorption has been proven to be a highly effective technique for the removal of heavy metals from waste streams [16-20].

Adsorption is the process through which a substance, originally present in one phase, is removed from that phase by accumulation at the interface between that phase and a separate (solid) phase. With adsorption, there is a wide variety of target pollutants, high capacity, fast kinetics and possibly selective depending on adsorbent [15-16]. The adsorption process can take place in systems such as liquid-gas, liquid-liquid, solid-liquid and solid-gas. The adsorbing phase is the *adsorbent*, and the material concentrated or adsorbed at the surface of the adsorbing phase is the *adsorbate* [21].

Various materials have been used as adsorbents for the removal of heavy metals. These adsorbents include zeolites [22-25], activated carbon [26-29], modified silica gel [30-32] and natural fibres [33-37]. Zeolites, activated carbon (except when natural fibres are used for the production of activated carbon) and modified silica gel are expensive and they are not environmentally friendly. A number of studies have shown that natural fibres can be used as an alternative for removing metals in contaminated water [33-37]. This was attributed to the low cost, low density, high availability and environmental friendliness of natural fibres. Moreover, natural fibres require little processing and are selective adsorbents of heavy metals.

A number of studies have reported on the removal of heavy metals using sugarcane bagasse (SCB) [38-41]. SCB is a fibrous material left after the crushing of cane stalk and juice extraction. Structurally, sugarcane is composed of an outer rind and inner pith. The majority of sucrose together with bundles of small fibres are found in the inner pith. The outer rind contains longer and finer fibres, in a random arrangement throughout the stem and bound together by lignin and hemicelluloses. Sugarcane bagasse is a lignocellulosic plant waste which is composed of cellulose, hemicellulose, lignin, pectin, waxes, water-soluble substances, and moisture [40]. It is used as a metal adsorbent due to (i) benign lignocellulosic material, (ii) inexpensive (sugarcane industry waste), and (iii) rich in oxygen containing functional groups such as phenols and carbonyls. It has pronounced capability for uptake of heavy metals in aqueous solution with no need of chemical modification. The main problem regarding the use of natural fibres like SCB as adsorbents is that they are easily degraded by microbes when in aqueous medium and they cannot be used for a long period of time [42]. Therefore there is a need to protect or mask fibres against bacterial contact.

Thermoplastic, thermosets and biodegradable polymers have been widely used as matrices (masking agents) for various applications. These applications include structural (automotive), packaging and other areas of composites [43-47], but less work has been done on composites for water purification. Biodegradable matrices offer many advantages over their counterparts, which lately give them wide application in composite technology. Biodegradable polymers are plastics obtained from renewable resources synthesized from petroleum-based chemicals and they are environmentally friendly, fully degradable and sustainable. Biodegradable polymers such as poly(lactic acid) (PLA), poly(ϵ -caprolactone) (PCL), thermoplastic starch (TPS) and polybutylene succinate adipate copolymer (PBSA) have been used by numerous researchers [48-50]. PLA displays a variety of characteristics which enable its use as a polymer matrix for fibre composites. It is a hydrophobic synthetic polymer made from renewable agricultural feedstock (corn starch) through fermentation followed by the polymerization of lactic acid. Its characteristics include: environmental friendliness, biocompatibility, ease processability and less energy dependence. Despite its advantages, PLA cannot be used in certain applications due to its hydrophobic nature, brittleness and poor toughness. The disadvantages of PLA can be improved by blending with flexible polymers or addition of filler [48].

Production of polymeric material from existing polymers is an important method and is called polymer blending. A mixture of at least two polymers or copolymers is known as a polymer blend. The advantages of polymer blending include cost effectiveness and less time-consumption than the development of new monomers as the basis for new polymeric materials. Additionally, a wide range of material properties is within reach by merely changing the blend composition. Polymer blending is performed to improve polymer properties such as mechanical strength, biocompatibility and thermal stability that individual polymers do not possess. Many studies have been done on the polymer blending of PLA with other polymers such as polypropylene, ethylene vinyl acetate and poly(butylenes adipate-co-terephthalate) [41-55]. Ethylene vinyl acetate (EVA) is a good candidate to be blended with PLA since it has excellent flexibility, fracture toughness, adhesion to other organic/inorganic materials with long life time. However, due to their incompatibility, EVA and PLA cannot be successfully blended without significant reduction in mechanical properties. Hence, dicumyl peroxide (DCP) was used to improve the interaction between EVA and PLA, aiming to produce materials with improved properties.

In this study PLA/EVA/SCB composites were prepared for the removal of lead metal ions from aqueous media. However, SCB is incompatible with non-polar hydrophobic polymers due to their polar and hydrophilic nature, the incompatibility of hydrophilic and hydrophobic polymers is well documented [56-58]. This incompatibility leads to weak interfacial adhesion and non-uniform dispersion of the filler within the matrix during compounding. Due to the weak filler-matrix interaction, a decrease in the mechanical properties with its incorporation is one of the inherent problems [57]. To overcome this problem, several strategies have been proposed to enhance the adhesion between the natural fibre and the polymer matrix. These strategies generally involve modifications of the fibre and/or the matrix by physical or chemical methods. Chemical modification of the natural fibres includes: acetylation, mercerization, cyanoethylation, peroxide treatments, graft copolymerization (methylmethacrylate, acrylamide, and acrylonitrile) as well as various coupling agents (silane, isocyanate and titanate based compounds) [58-60]. Among all these methods, mercerization has shown a better compatibilization effect in polymer matrix based natural fibres [61-64].

In this study, SCB which is the residue left after crushing sugarcane stalks for the extraction of the sucrose-rich juice, has been selected because it is a highly promising metal adsorbent [65]. This is so because sugarcane is highly productive, abundant and contains functional groups that are responsible for metal complexation or ion-exchange [66]. The metal adsorption efficiency of PLA/EVA/SCB biocomposites was investigated by flame atomic absorption spectroscopy (AAS). This technique is preferred because of its specificity, sensitivity, precision, simplicity and relatively low cost per analysis [67]. To our knowledge, there are no reports on PLA/EVA/SCB bio-composites and it is important to understand their effect on the removal of heavy metals from aqueous media.

1.2 Literature review

1.2.1 Natural fibres: Sources and classification

Natural fibres are raw materials directly obtainable from animal, vegetable, or mineral sources. Vegetable fibres are extracted from plants and are classified into three categories, depending on

the part of the plant they are extracted from. (1) Fruit fibres are extracted from the fruits of the plant, they are light and hairy, and allow the wind to carry the seeds. (2) Bast fibres are found in the stems of the plant providing the plant its strength. Usually they run across the entire length of the stem and are therefore very long. (3) Fibres extracted from the leaves are rough and sturdy and form part of the plant's transportation system, they are called leaf fibres. Natural fibres were and still are the basis for producing clothes, papers, tools, and building materials. They are rigid, crystalline cellulose microfibril-reinforced amorphous lignin and/or hemicellulose matrices. Natural fibres are cheap, non-abrasive, have low density, abundant, low energy consumption, biodegradable, recyclable and renewable [57].

1.2.2 Properties of natural fibres

Properties as well as the quality of a fibre depend on factors such as maturity and the processing methods adopted for the extraction of the fibres. An increase in diameter of a fibre results in a decrease in modulus. Properties such as density, electrical resistivity, ultimate tensile strength and initial modulus are related to the internal structure and chemical composition of the fibres. The smaller the angle between the axis and the fibre fibrils, the better the mechanical properties, i.e. the strength and stiffness of the fibre. These properties are also considerably affected by the chemical constituents and complex chemical structure of natural fibres. Cellulose content and microfibrillar angle cannot be correlated with fibre strength, because of the very complex structure of natural fibres. Filament and individual fibre properties can vary widely depending on various factors such as source, age, separating technique, moisture content, history of the fibre and speed of testing [57,68-96].

Plant or lignocellulosic fibres are considered as naturally occurring composites consisting mainly of cellulose fibrils embedded in a lignin matrix. The main constituents of the plant fibres are cellulose, hemicellulose, and lignin with other constituents like pectins, waxes, water-soluble substances, and moisture [42,57,68-72]. The chemical composition of lignocellulosic fibres depends on various factors such as species, variety, type of soil used, weather conditions, part from which the fibres are extracted, and age of the plants [73].

Cellulose is a natural polymer made by linking of smaller molecules (Figure 1.1). The links in the cellulose chain consist of sugar, β -D-glucose. The sugar units are linked when water is eliminated by combining the H and $-OH$ group. Linking just two of these sugars produces a disaccharide called cellobiose. In the cellulose chain, the glucose units are in 6-membered rings, called pyranoses. They are joined by single oxygen atoms (acetal linkages) between the C-1 of one pyranose ring and the C-4 of the next ring. Since a molecule of water is lost due to the reaction of an alcohol and a hemiacetal to form an acetal, the glucose units in the cellulose polymer are referred to as anhydroglucose units. The cellulose molecular structure is the reason for its hydrophilicity, chirality, degradability, and its unique reactivities. Cellulose is easily hydrolyzed by acids to water-soluble sugars, but is resistant to strong alkali [42,57,68-72].

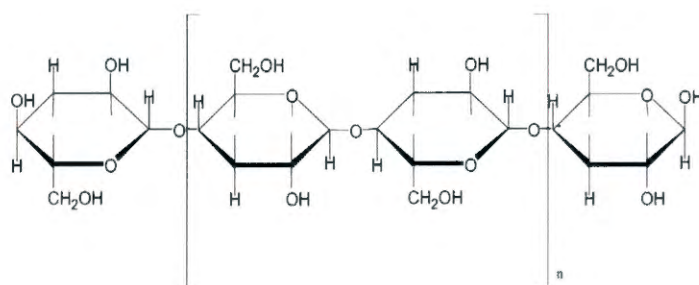


Figure 1.1 Chemical structure of cellulose [72]

Hemicellulose consists of linear homo- or copolymers of variable degree of branching (usually single monosaccharidic branches) and with occasional (3-13 wt. %) replacement of OH groups by O-acetyl groups (Figure 1.2). It contains a group of polysaccharides compiled of five and six carbon ring sugars. It differs from cellulose in three aspects, firstly, it contains several sugar units; secondly they exhibit a considerable degree of chain branching containing pendent side groups giving rise to its ion crystalline nature. The third aspect is its degree of polymerization, which is 30-50, 10-100 times less than that of cellulose. Hemicellulose is very hydrophilic, soluble in alkali and easily hydrolyzed in acids [42,57,68-72].

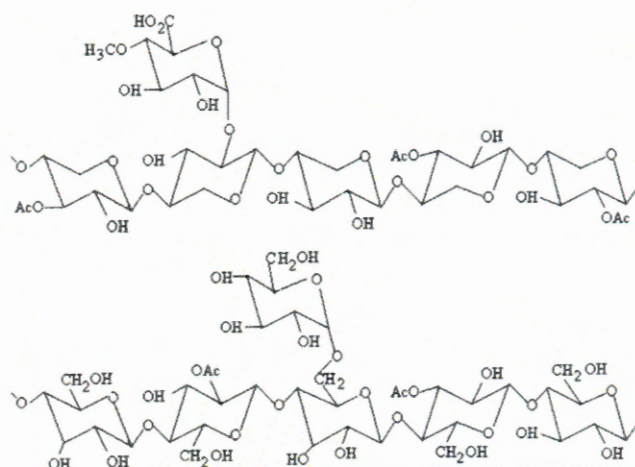


Figure 1.2 Chemical structure of hemicellulose [72]

Lignin is a complex hydrocarbon polymer with both aliphatic and aromatic constituents, and it is totally insoluble in most of the solvents and cannot be broken down into monomeric units (Figure 1.3). Lignin is considered to be a thermoplastic polymer having a glass transition temperature of around 90 °C and a melting temperature of around 170 °C. It is totally amorphous and hydrophobic in nature. It can be hydrolyzed by acids, but it is soluble in hot alkali, readily oxidized and easily condensable with phenol. The structure, properties and morphology of the fibre is influenced by the lignin content [42,57,68-72].

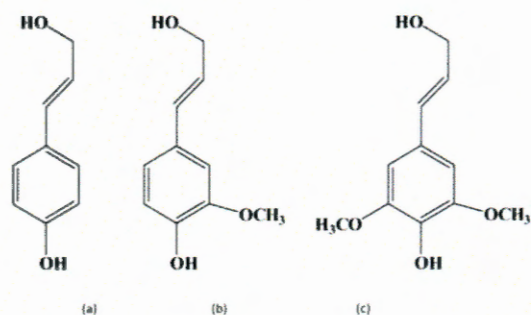


Figure 1.3 Chemical structure of lignin [72]

Pectin is a collective name for heteropolysaccharides and they provide flexibility to plants. They are soluble in water only after a partial neutralization with alkali or ammonium hydroxide [42,57,68-72].

Wax consists of different types of alcohols, which are insoluble in water as well as several acids (palmitic acid, oleaginous acid and stearic acid). The part of the fibres which can be extracted with organic solutions is made up of wax. Wax generally influences the wettability as well as the adhesion characteristics of the fibres [42,68-73].

1.2.2.1 Structure, physical, and mechanical properties of natural fibres

A single fibre of all plant based natural fibres consists of several cells. The structure and the properties of natural fibres are determined and influenced by the dimensions and the arrangements of unit cells in a fibre. The dimensions of individual cells in natural fibres are dependent on the species, maturity and location of the fibres in the plant and also on the fibre extraction conditions. These cells are formed out of crystalline microfibrils based on cellulose, which are connected to a complete layer by amorphous lignin and hemicellulose. The diameter of these microfibrils ranges from 10 to 30 nm, and each microfibril is made up of 30-100 cellulose molecules in extended chain conformation. Every fibril has a complex, layered structure consisting of a thin primary wall that is the first layer deposited during cell growth encircling a secondary wall. The secondary wall is made up of three layers, and the thick middle layer determines the mechanical properties of the fibre. The middle layer consists of a series of helically wound cellular microfibrils formed from long chain cellulose molecules as seen in Figure 4. The angle between the fibre axis and the microfibrils is called the microfibrillar angle. The characteristic value for this parameter varies from one fibre to another. The spiral angle of the fibrils and the content of cellulose generally determine the mechanical properties of the cellulose based natural fibres. There are several physical properties that are important to know about for each natural fibre, before that fibre can be used to reach its highest potential. These properties include fibre dimensions, defects, strength, variability, crystallinity, and structure [57,68-69,71].

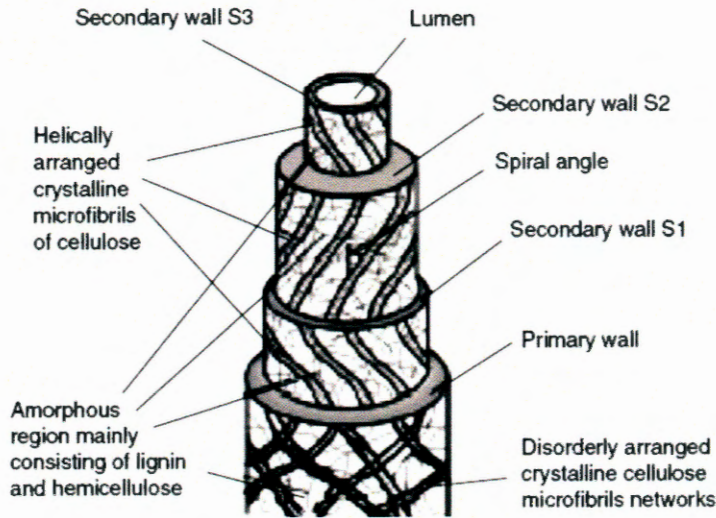


Figure 1.4 Structure of natural fibre cell [68]

The properties of a fibre such as tensile strain, tensile stress, specific tensile modulus, and specific tensile strength were evaluated as a function of geometrical variation, extraction method and the diameter of the fibres [74]. It was found that the density of various natural fibres are likely to vary depending on the process of fibre extraction, age of the plant, moisture present in the fibre and the soil condition in which the plant has grown. It was observed that the failure of fibres in tension is due to pull-out of microfibrils accompanied by tearing of cell walls. The tendency of fibre pull-out decreases with increasing speed of testing. Generally it was observed that an increase in cellulose content results in an increase in tensile strength and the Young's modulus of the fibres. The stiffness of the fibres is determined by the microfibrillar angle [75].

1.2.3 Sugarcane bagasse (SCB)

SCB is a fibrous residue which remains after sugarcane (*Saccharum officinarum*) stalks are crushed to extract their juice. SCB which has short renewal times, wide availability, biodegradability, ease of cultivation and low cost, associated with excellent physical and mechanical characteristics, is currently the most widely used natural fibre. It is currently used as a renewable natural fibre for the manufacture of composites materials [44]. The SCB as well as any other types of plant biomass is composed by cellulose, hemicellulose, lignin, and small amounts

of extractives and mineral salts. Sugarcane stalk is made up of shorter segments and joints. Each joint consists of two distinctive parts i.e. node and internode. The cross-section of the internode is composed of the rind (outer layer) and the pith (inner layer). The majority of sucrose along with bundles of small fibres is found in the pith. The rind consists of numerous longer and finer fibre bundles composed of elemental fibres in discrete elongated units embedded in a matrix of lignin and hemicellulose. These elemental fibres are bound together by an amorphous matrix of lignin and hemicellulose to form fibre bundles [76-78].

1.2.3.1 Chemical composition of SCB

The chemical composition of SCB fibres have been reported by many researchers [79-83]. These researchers found varied contents of cellulose (40-50%), hemicellulose (24-35%), lignin (20-30%) and small amounts of ash and acetyl groups. This variation in chemical composition of SCB fibres was attributed to the fact that the chemical composition of lignocellulosic fibres depends on various factors such as species, variety, type of soil used, weather conditions, part from which the fibres are extracted, and age of the plant [76,77].

1.2.3.2 Thermal properties of SCB

The thermal properties of SCB fibres have been studied by a number of researchers using thermogravimetric analysis (TGA) [84-87]. The results of the weight loss of SCB fibres as a function of temperature for these studies can be summarized as follows: the first small change in weight up to 100 °C was related to water loss associated with moisture present in the SCB. Between 100 and 200 °C, the SCB was thermally stable. Between 200 and 300 °C, the weight loss was about 10%. From 300 to 400 °C, the fibre displayed considerable mass loss (more than 70%) due to decomposition of both cellulose and hemicellulose. Above 400 °C, degradation of fibres can be attributed to the breakage of bonds of the lignin. Above 500 °C, only about 1% ash was observed. Therefore, 200 °C can be considered as the maximum temperature up to which SCB fibres can be used.

1.2.4 Composite properties

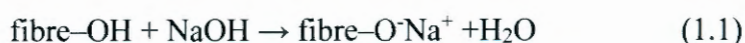
Composites consist of one or more discontinuous phases embedded in a continuous phase. The discontinuous phase is usually harder and stronger than the continuous phase and is called the 'reinforcement' or 'reinforcing material', whereas the continuous phase is termed as the 'matrix'. Properties of composites are strongly dependent on the properties of their constituent materials, their distribution and the interaction between them. The composite properties may be the volume fraction sum of the properties of the constituents or the constituents may interact in a synergistic way resulting in improved or better properties. Apart from the nature of the constituent materials, the geometry of the reinforcement (shape, size and size distribution) influences the properties of the composite to a large extent. The concentration distribution and orientation of the reinforcement also affect the properties.

1.2.4.1 Modification of polymer/natural fibre composites

Composites based on natural fibres are an interesting alternative when moderate mechanical properties are required. Since the interfacial bonding between the reinforcing fibres and the polymer matrix is an important element in realizing the mechanical properties, several authors [57,70,71,88-91] focused their studies on the treatment of fibres to improve the bonding with the polymer matrix. The mechanical properties of the composites are controlled by the properties and quantities of the component materials and by the character of the interfacial region between the matrix and reinforcement. Lack of good interfacial adhesion makes the use of cellular fibre composites less attractive. Natural fibre composites combine good mechanical properties with low specific mass, but their high level of moisture absorption, poor wettability and insufficient adhesion between the untreated fibre and the polymer matrix leads to debonding with age. To improve the properties of the composites, it is necessary to improve the adhesion between the hydrophilic fibre and the hydrophobic matrix by modifying the fibre surface. Natural reinforcing fibres can be modified by physical and chemical methods. Physical modification changes the structural and surface properties of the fibre, thereby influencing the mechanical bonding with the matrix. The chemical modification of the fibres alters the surface properties so that better wetting of the fibres with the matrix is possible. This removes the organic residues from the surfaces of

the fibres which enhances the adhesion, because natural fibres are coarse in structure, and thus enable an interlocking mechanism with the matrix. According to the principles of interface coupling, the hydrophilic carboxyl group of an organic acid as a modifier is expected to react with the hydroxyl groups on the surface of natural fibre, and the hydrophobic group should react or have relatively high compatibility with the polymer matrix. The combined effects of these interactions will effectively improve the fibre dispersion and resultant adhesive coupling. There are various chemical treatments available for the fibre surface modification. Chemical treatment includes alkali, silane, acetylation, benzylation, acrylation, isocyanates, maleated coupling agents and permanganate treatment.

Alkaline treatment or mercerization is one of the most used chemical treatments of natural fibres when used to reinforce thermoplastics and thermosets. The important modification done by alkaline treatment is the disruption of hydrogen bonding in the network structure, thereby increasing surface roughness. This treatment removes a certain amount of lignin, wax and oils covering the external surface of the fibre cell wall, depolymerizes cellulose and exposes the short length crystallites. Addition of aqueous sodium hydroxide (NaOH) to natural fibre promotes the ionization of the hydroxyl group to an alkoxide.



Thus, alkaline processing directly influences the cellulosic fibril, the degree of polymerization and the extraction of lignin and hemicellulosic compounds. It was reported that alkaline treatment had two effects on the fibre 1) It increased surface roughness resulting in better mechanical interlocking, and 2) it increased the amount of cellulose exposed on the fibre surface, therefore increasing the number of possible reaction sites [92].

1.2.4.2 Morphologies of polymer blends/natural fibre composites

Improved interfacial adhesion usually leads to better fibre dispersion and transfer of stress from one phase to the other. Several methods have been reported for improving the interfacial compatibility between hydrophilic cellulosic fibres and hydrophobic polymer matrices

[57,70,71,88-91]. The influence of these modification methods in the morphologies and interfacial properties of polymer blends reinforced natural fibre composites have been investigated by several researchers [93-98], and compared with their unmodified counterparts. It was generally observed that the interfacial bonding between the fibre and the polymer blend improved when the fibre surfaces were treated with chemical or physical treatments, when only the polymer matrix was modified, or when both of them were modified. The untreated composites, on the other hand, showed poor interfacial adhesion, as the existence of fibre pull-out from the matrix material during fracture, and their surfaces remained practically clean. Moreover, the absence of any physical contact between the fibre and the matrix was also detected.

1.2.4.3 Mechanical properties of polymer blends/natural fibre composites

Mechanical properties of polymer blends/natural fibre composites were reported in a number of papers [93-98]. It was generally found that the Young's moduli and tensile strength of the polymer blends/natural fibre composites were dependent on the improved dispersion and interfacial adhesion. Well dispersed composites resulted in an increase in Young's moduli as well as an increase in tensile strength. This was due to the presence of well dispersed additional reinforcement structures that make the matrix tougher. Elongation at yield and yield stress did not show similar trends, but varied according to the investigated polymer blends/natural fibre composites. The decrease in elongation at yield was due to decrease in the flexibility of the composite due to the addition of the filler. It was generally seen that the % elongation at break point decreases with the addition of fillers, despite the state of the interface between the different phases. Natural fibres are generally known to increase stiffness which in turn enhances modulus of composites when they are used as reinforcement. Generally, it was found that the impact strength of polymer blend composites decreases as the fibre content increases. The decrease in impact strength as fibre content increases was attributed to fibre bundle or agglomerate formation which reduces the transfer of the external forces between fibre and the matrix. It was also reported that the mechanical properties of natural fibre-polymer blend composites depend on several other factors such as the type of cellulosic fibres, fibre length, loading, and orientation, as well as the processing conditions during composite preparations [99]. It can be concluded that untreated composites usually have

poor mechanical properties than the blends or treated composites due to poor interfacial bonding between the fibre and the polymer blend matrix.

1.2.5 Water absorption of polymer/natural fibre composites

Moisture penetration into composite materials is conducted by three different mechanisms as reported by many researchers [100-103]. The main process consists of diffusion of water molecules inside the micro-gaps between polymer chains. The other common mechanisms are capillary transport into the gaps and flaws at the interfaces between fibres and polymer, because of the incomplete wettability and impregnation; and transport by micro-cracks in the matrix formed during the compounding process. In general, diffusion behaviour in polymers can be classified according to the relative mobility of the penetrant and of the polymer segments. The capillary mechanism involves the flow of water molecules into the interface between fibres and matrix. It is particularly important when the interfacial adhesion is weak and when the debonding of the fibres and the matrix has started. On the other hand, transport by micro-cracks includes the flow and storage of water in the cracks, pores or small channels in the composite structure.

Several researchers [104-106] reported that natural fibre-polymer composites has high water uptake compared to neat polymer matrices, which showed that polymers have little water absorption effect. Thermoplastic and bio-degradable polymers are hydrophobic in nature and therefore would reduce water uptake in the composites. Water absorption effect on composites increased with an increase in fibre content. This was attributed to the hydrophilic nature of the natural fibres resulting into poor interfacial bonding with hydrophobic thermoplastics thus allowing water penetration through the composite materials. An increase in hydrophilic natural fibre content results into a less hydrophobic thermoplastic material to encapsulate fibres and therefore increased water uptake.

1.2.6 Adsorption

Adsorption is a process of binding molecules or particles onto the external surface of solid or internal surface if the material is porous in a very thin layer. Adsorption process proceeds in three

steps: i) Transfer of the adsorbate molecules through the film that surrounds the adsorbent. ii) Diffusion through the pores if the adsorbent is porous. iii) Uptake of the adsorbate molecules by active surface, including formation of the bond between the adsorbate and the adsorbent. Adsorption can occur in two ways which are the chemisorption and physisorption. In chemisorption the forces involved are valence forces of the same kind as those operating in the formation of chemical compounds. Chemisorption is favoured at high temperature because chemical reactions proceed more rapidly at an elevated temperature. With physisorption the forces that are involved are intermolecular forces (van der Waals forces) of the same kind as those responsible for the imperfection of real gases and the condensation of vapours. These forces do not involve a significant change in the electronic orbital patterns of the species involved. In physisorption, adsorbed molecules are not attached to a specific site at the surface of adsorbent but are free to undergo translational movement within the interface. It is predominant at low temperature and is characterized by relatively low energy of adsorption. The rate of adsorption depends on the rate at which the molecules move by diffusion in solution or the rate at which the molecules can reach available surface by diffusing through the film and the pores. Adsorption capacity depends on the physical and chemical characteristics of both the adsorbent and adsorbate, the concentration of the adsorbate in liquid solution, the experimental conditions such as temperature and solution pH, and the amount of time the adsorbate is in contact with the adsorbent [107].

1.2.6.1 Uses of natural fibres as adsorbents in water treatment

There were a fair number of studies on the use of natural fibres as adsorbents of heavy metals [108-114]. The removal of metal ions from aqueous media using natural fibres is based on metal biosorption. The process of biosorption involves a solid phase (sorbent) and a liquid phase (solvent) containing a dissolved species to be sorbed. Due to a high affinity of the sorbent for the metal ion species, the latter is attracted and bound by a complex process affected by several mechanisms. These mechanisms involve chemisorption, complexation, adsorption on the surface and pores, ion exchange, chelation, adsorption by physical forces, entrapment in inter and intrafibrillar capillaries and spaces of the structural polysaccharides network as a result of the concentration gradient and diffusion through the cell wall and membrane. Natural fibres are

composed of many constituents; amongst these constituents are functional groups that have the affinity for metal complexation. These functional groups present in natural fibres include acetamido, carbonyl, phenolic, structural polysaccharides, amido, amino, sulphhydryl carboxyl groups, alcohols and esters.

There are a number of parameters that have been reported when using natural fibres as adsorbents [104-114]. These parameters include pH level of the solution, contact time between the adsorbent and the adsorbate, temperature of the solution, the amount of the adsorbent and the initial concentration of the solution. It was generally found that the adsorption efficiency increased with an increase in pH level. However, it was found that at lower pH levels the removal efficiency was very low because of the large number of hydronium ions (H_3O^+) in the solution. Metal ions have to compete with these hydronium ions for the adsorbent sites. It was also found that the functional groups in natural fibres were protonated at lower pH levels and hence rendered unavailable for ion exchange and complexation with the metal ions. At pH levels of 3 to 7 the adsorption efficiency was very high due to less competition, resulting in large numbers of adsorption sites in the adsorbate. These investigations also showed that at pH levels higher than 7, metal ions start to precipitate which defeats the very purpose of employing adsorption. Adsorption of heavy metals by natural fibres was found to initially increase with an increase in contact time until it reaches equilibrium i.e. there are no more available sites on the adsorbent. It was generally observed that the percentage removal of heavy metals decreased with an increase in initial concentration. At lower concentration, most of the metal solution will react with the binding sites due to the larger surface area of the adsorbent, and thus facilitate almost complete sorption. At higher concentrations, more metal ions were left unabsorbed in the solution due to the saturation of the binding sites. However, Putra *et al.* [114] found that the significant amount of metal ions adsorbed at high initial metal concentrations can be related to two main factors: i) probability of collision between metal ions with the bio-sorbent surface, and ii) high rate of metal ions diffusion onto the bio-sorbent surface. It was also seen from these results that the removal efficiency increased rapidly with an increase in bio-sorbent, which was attributed to increased surface area of the bio-sorbent and the availability of more binding sites due to increased amount of bio-sorbent.

1.2.6.2 Adsorption isotherms

Adsorption isotherms represent the relationship between the amount adsorbed by a unit weight of solid sorbent and the amount of solute remaining in the solution at equilibrium. The Langmuir and Freundlich isotherm models are frequently used for describing short term and mono component adsorption of metal ions by different materials. Simplicity and easy interpretability are some of the reasons for the extensive use of these models. A number of reports were published on these models [115-121]. To calculate the adsorption capacity of metal ions on the fibres at equilibrium, q_e is calculated according to Equation 1.2.

$$q_e = \frac{(C_o - C_e)V}{m} \quad (1.2)$$

where V is the volume of the solution and m is the mass of sorbent used. C_o (mg L^{-1}) and C_e (mg L^{-1}) are the initial and equilibrium concentrations of the metal ions.

Langmuir adsorption isotherm

The Langmuir isotherm, also called the ideal localized monolayer model, was developed to represent chemisorption. Langmuir theoretically examined the adsorption of gases on solid surfaces, and considered sorption as a chemical phenomenon. The Langmuir equation relates the coverage of molecules on a solid surface to concentration of a medium above the solid surface at a fixed temperature. This isotherm is based on the assumption that adsorption is limited to monolayer coverage, all surface sites are alike and can only accommodate one adsorbed molecule, the ability of a molecule to be adsorbed on a given site is independent of its neighbouring sites' occupancy, adsorption is reversible and the adsorbed molecule cannot migrate across the surface or interact with neighbouring molecules. By applying these assumptions and the kinetic principle (rate of adsorption and desorption from the surface is equal), the Langmuir equation can be written in a hyperbolic form Equation 1.3.

$$q_e = q_m \frac{K_L C_e}{1 + K_L C_e} \quad (1.3)$$

where q_e is the adsorption capacity at equilibrium (mg g^{-1}), q_{max} is the theoretical maximum adsorption capacity of the adsorbent (mg g^{-1}) and, as such, can be thought of as the best criterion for comparing adsorptions, K_L is the Langmuir affinity constant (L mg^{-1}) and C_e is the supernatant equilibrium concentration of the system (mg L^{-1}). This isotherm equation has been most frequently applied in equilibrium studies of adsorption, but it should be realized that the Langmuir isotherm offers no insights into aspects of adsorption mechanisms.

Freundlich adsorption isotherm

The Freundlich isotherm was originally of an empirical nature, but was later interpreted as sorption onto heterogeneous surfaces or surfaces supporting sites of varied affinities. It is assumed that the stronger binding sites are occupied first and that the binding strength decreases with increasing degree of site occupation. The Freundlich isotherm can describe the adsorption of organic and inorganic compounds on a wide variety of adsorbents. According to this model the adsorbed mass per mass of adsorbent can be expressed by a power law function of the solute concentration as in Equation 1.4.

$$q_e = K_F C_e^{\frac{1}{n}} \quad (1.4)$$

where K_F is the Freundlich constant related to adsorption capacity (mg g^{-1}) and n is the heterogeneity coefficient (dimensionless). For linearization of the data, the Freundlich equation is written in logarithmic form Equation 1.5.

$$\log q_e = \log K_F + \left(\frac{1}{n}\right) \log C_e \quad (1.5)$$

The plot of $\log q_e$ versus $\log C_e$ has a slope equal to $1/n$ and an intercept equal to $\log K_F$. On average, a favourable adsorption tends to have a Freundlich constant n between 1 and 10. Larger values of n imply stronger interaction between the adsorbent and the adsorbate, while $1/n$ equal to 1 indicates linear adsorption leading to identical adsorption energies for all sites. Linear adsorption generally occurs at very low solute concentrations and low loading of the adsorbent.

1.3 Aims and objectives

- The main aim of this study was to formulate effective and environmentally friendly PLA/EVA/SCB biocomposites for the removal of lead (Pb).
- To study the thermal properties of the composites using thermogravimetric analysis to understand the influence of the presence and amount of filler on the thermal stability of the biocomposites.
- To study the morphologies and the interfacial adhesion between the polymers and the filler by using scanning electron and optical microscopy.
- To determine the impact properties of the composites in order to establish their durability during use.
- To test the effectiveness of the biocomposites for heavy metal removal through atomic absorption spectroscopy (AAS).
- To investigate the effect of contact time, pH level, and initial concentration on biocomposites.
- To use the Langmuir and Freundlich adsorption isotherms to interpret the adsorption behaviour of lead ions onto the bio-composites.

1.4 Thesis outline

The outline of this thesis is as follows:

- Chapter 1: General introduction and literature review
- Chapter 2: Materials and methods
- Chapter 3: Results and discussion
- Chapter 4: Conclusions

1.5 References

- [1] W. Li, L. Zhang, J. Peng, N. Li, S. Zhang, S. Guo. Tobacco stems as a low cost adsorbent for the removal of Pb(II) from wastewater: Equilibrium and kinetic studies. *Industrial Crops and Products* 2008; 28:294-302.
DOI:10.1016/j.indcrop.2008.03.007

- [2] U. Garg, M.P. Kaur, G.K. Jawa, D. Sud, V.K. Garg. Removal of cadmium (II) from aqueous solutions by adsorption on agricultural waste biomass. *Journal of Hazardous Materials* 2008; 154:1149-1157.
DOI: 10.1016/j.jhazmat.2007.11.040
- [3] E. Pehlivan, T. Altun, S. Cetin, M.I. Bhangar. Lead sorption by waste biomass of hazelnut and almond shell. *Journal of Hazardous Materials* 2009; 167:1203-1208.
DOI:10.1016/j.jhazmat.2009.01.126
- [4] K.P. Patil, V.S. Patil, P. Nilesh, V. Motiraya. Adsorption of copper (Cu²⁺) & zinc (Zn²⁺) metal ion from waste water by using soybean hulls and sugarcane bagasse as adsorbent. *International Journal of Scientific Research and Reviews* 2012; 1:13-23.
- [5] A. Ahmad, M. Rafatullah, O. Sulaiman, M.H. Ibrahim, Y.Y. Chii, B.M. Siddique. Removal of Cu(II) and Pb(II) ions from aqueous solutions by adsorption on sawdust of Meranti wood. *Desalination* 2009; 247:636-646.
DOI: 10.1016/j.desal.2009.01.007
- [6] H.A. Qdais, H. Moussa. Removal of heavy metals from wastewater by membrane processes: A comparative study. *Desalination* 2004; 164:105-110.
DOI: 10.1016/S00119164(04)00169-9
- [7] M.I. Ansari, F. Masood, A. Malik. Bacterial biosorption: A technique for remediation of heavy metals. *Microbes and microbial technology* 2011; 283-319.
DOI: 10.1007/978-1-4419-7931-5_12
- [8] B.Y. Gao, H.H. Hahn, E. Hoffmann. Evaluation of aluminium-silicate polymer composite as a coagulant for water treatment. *Water Research* 2002; 36:3573-3581.
DOI: 10.1016/S0043-1354(02)00054-4
- [9] J. Jiang, B. Lloyd. Progress in the development and use of ferrate(VI) salt as an oxidant and coagulant for water and wastewater treatment. *Water Research* 2002; 36:1397-1408.
DOI: 10.1016/S0043-1354(01)00358-X
- [10] L. Charerntanyarak. Heavy metals removal by chemical coagulation and precipitation. *Water Science and Technology* 1999; 39:135-138.
DOI: 10.1016/S0273-1223(99)00304-2
- [11] T.R. Harper, N.W. Kingham. Removal of arsenic from wastewater using chemical precipitation methods. *Water Environmental Research* 1992; 64:200-203.

DOI: 10.2175/WER.64.3.2

- [12] R.J. Stephenson, S.J.B. Duff. Coagulation and precipitation of a mechanical pulping effluent-I. Removal of carbon, colour and turbidity. *Water Research* 1996; 30:781-792.
DOI: 10.1016/0043-1354(95)00213-8
- [13] M.A. Sabur, A.A. Khan, S. Safiullah. Treatment of textile wastewater by coagulation precipitation method. *Journal of Scientific Research* 2012; 4:623-633.
DOI: 10.3329/jsr.v4i3.10777
- [14] A. Shukla, Y. Zhang, P. Dubey, J.L. Margrave, S.S. Shukla. The role of sawdust in the removal of unwanted materials from water. *Journal of Hazardous Materials* 2002; 95:137-152.
DOI: 10.1016/S0304-3894(02)00089-4
- [15] D.W. O'Connell, C. Birkinhaw, T.F O'Dwyer. Heavy metal adsorbents prepared from the modification of cellulose: A review. *Bioresource Technology* 2008; 99:6709-6724.
DOI: 10.1016/j.biortech.2008.01.036
- [16] N.A. Khan, S. Ibrahim, P. Subramaniam. Elimination of heavy metals from wastewater using agricultural wastes as adsorbents. *Malaysian Journal of Science* 2004; 23:43-51.
- [17] E. Omar, S. Abdel, N.A. Reiad, M.M. ElShafei. A study of the removal characteristics of heavy metals from wastewater by low-cost adsorbents. *Journal of Advanced Research* 2011; 2:297-303.
DOI: 10.1016/j.jare.2011.01.008
- [18] D. R. Mulinari, M.L.C.P. da Silva. Adsorption of sulphate ions by modification of sugarcane bagasse cellulose. *Carbohydrate Polymers* 2008; 74:617-620.
DOI: 10.1016/j.carbpol.2008.04.014
- [19] W.P. Putra, A. Kamari, S.N.M. Yusoff, C.F. Ishak, A. Mohamed, N. Hashim, I. Md Isa. Biosorption of Cu(II), Pb(II) and Zn(II) ions from aqueous solutions using selected waste materials: Adsorption and characterisation study. *Journal of Encapsulation and Adsorption Science* 2004; 4:25-35.
DOI: 10.4236/jeas.2014.41004
- [20] R. Lakshmipathy, N.C. Sarada. Adsorptive removal of basic cationic dyes from aqueous solution by chemically protonated watermelon (*Citrullus lanatus*) rind biomass. *Desalination and Water Treatment* 2013; 52:6175-6184.

DOI: 10.1080/19443994.2013.812526

- [21] U. Singh, R.K. Kaushal. Treatment of waste water with low cost adsorbent: A review. *VSRD International Journal of Technical and Non-Technical Research* 2013; 4:33-42.
- [22] S.M. Shaheen, A.S. Derbalah, F.S. Moghanm. Removal of heavy metals from aqueous solution by zeolite in competitive sorption system. *International Journal of Environmental Science and Development* 2012; 3:362-367.
DOI: 10.7763/IJESD.2012.V3.248
- [23] S. Mehdizadeh, S. Sadjadi, S.J. Ahmadi, M. Outokesh. Removal of heavy metals from aqueous solution using platinum nanoparticles/zeolite-4A. *Journal of Environmental Health Science and Engineering* 2014; 12:1-7.
DOI: 10.1186/2052-336X-12-7
- [24] N.A. Booker, E.L. Cooney, A.J. Priestley. Ammonia removal from sewage using natural Australian zeolite. *Water Science and Technology* 1996; 34:17-24.
DOI: 10.1016/S0273-1223(96)00782-2
- [25] M.M. Motsa, J.M. Thwala, T.A.M. Msagati, B.B. Mamba. The potential of melt-mixed polypropylene-zeolite blends in the removal of heavy metals from aqueous media. *Physical and Chemistry of the Earth* 2011; 36:1178-1188.
DOI: 10.1016/j.pce.2011.07.072
- [26] I. Uzun, F. Guzel. Adsorption of some heavy metal ions from aqueous solution by activated carbon and comparison of percent adsorption results of activated carbon with those of some other adsorbents. *Turkish Journal of Chemistry* 2000; 24:291-297.
- [27] H. Tavallali, A. Daneshyar. Chemically modified activated carbon with ethylenediamine for selective solid -phase extraction of Cr (III) and Fe (III). *International Journal of ChemTech Research* 2012; 4:1163-1169.
- [28] O.S. Amuda, A.A. Giwa, I.A. Bello. Removal of heavy metal from industrial wastewater using modified activated coconut shell carbon. *Biochemical Engineering Journal* 2007; 36:174-181.
DOI: 10.1016/j.bej.2007.02.013
- [29] E. Bernard, A. Jimoh, J.O. Odigure. Heavy metals removal from industrial wastewater by activated carbon prepared from coconut shell. *Research Journal of Chemical Sciences* 2013; 3:3-9.

- [30] M. Li, M. Li, C. Feng, Q. Zeng. Preparation and characterization of multi-carboxyl-functionalized silica gel for removal of Cu (II), Cd (II), Ni (II) and Zn (II) from aqueous solution. *Applied Surface Science* 2014; 314:1063-1069.
DOI: 10.1016/j.apsusc.2014.06.038
- [31] R. Kumar, M.A. Barakat, Y.A. Daza, H.L. Woodcock, J.N. Kuhn. EDTA functionalized silica for removal of Cu(II), Zn(II) and Ni(II) from aqueous solution. *Journal of Colloid and Interface Science* 2013; 408:200-205.
DOI: 10.1016/j.jcis.2013.07.019
- [32] E. Repo, J.K. Warchol, A. Bhatnagar, M. Sillanpaa. Heavy metals adsorption by novel EDTA-modified chitosan-silica hybrid materials. *Journal of Colloid and Interface Science* 2011; 358:261-267.
DOI: 10.1016/j.jcis.2011.02.059
- [33] O.E.A. Salam, N.A Reiad, M.M. Elshafei. A study of the removal characteristics of heavy metals from wastewater by low-cost adsorbents. *Journal of Advanced Research* 2011; 2:297-303.
DOI:10.1016/j.jare.2011.01.008
- [34] D. Chaturvedi, O. Sahu. Adsorption of heavy metal ions from wastewater. *Global Journal of Environmental Science and Technology* 2014; 2:020-028.
- [35] M. Jaishankar, B.B. Mathew, M.S. Shah, K.T.P. Murthy, S.K.R. Gowda. Biosorption of few heavy metal ions using agricultural wastes. *Journal of Environment Pollution and Human Health* 2014; 2:1-6.
DOI: 10.12691/jephh-2-1-1
- [36] K.S. Geetha, S.L. Belagali. Removal of heavy metals and dyes using low cost adsorbents from aqueous medium-A review. *IOSR Journal of Environmental Science, Toxicology and Food Technology* 2013; 4:56-68.
DOI: 10.6084/m9.figshare.1188977
- [37] N.W. Ingole, V.N. Patil. Cadmium removal from aqueous solution by modified low cost adsorbent(s): A state of the art. *International Journal of Civil, Structural, Environmental and Infrastructure Engineering Research and Development (IJCSEIERD)* 2013; 3:17-26.
- [38] P.L. Homagai, K.N. Ghimire, K. Inoue. Adsorption behavior of heavy metals onto chemical modified sugarcane bagasse. *Bioresource Technology* 2010; 101:2067-2069.

DOI: 10.1016/j.biortech.2009.11.073

- [39] L.V.A. Gurgel, R.P. de Freitas, L.F. Gil. Adsorption of Cu(II), Cd(II), and Pb(II) from aqueous single metal solutions by sugarcane bagasse and mercerized sugarcane bagasse chemically modified with succinic anhydride. *Carbohydrate Polymers* 2008; 74:922-929. DOI: 10.1016/j.carbpol.2008.05.023
- [40] I. Ullah, R. Nadeem, M. Iqbal, Q. Manzoor. Biosorption of chromium onto native and immobilized sugarcanebagasse waste biomass. *Ecological Engineering* 2013; 60:99-107. DOI: 10.1016/j.ecoleng.2013.07.028
- [41] A. Kumar, O. Sahu. Sugar industry waste as removal of toxic metals from waste water. *World Journal of Chemical Education* 2013; 1:17-20. DOI: 10.12691/wjce-1-1-5
- [42] J.J. Maya, T. Sabu. Biofibres and bio-composites. *Carbohydrate Polymers* 2008; 71:343-364. DOI: 10.1016/j.carbpol.2007.05.040
- [43] M. Pracella, M.M. Haque, V. Alvarez. Functionalization compatibilization and properties of polyolefin composites with natural fibers. *Polymers* 2010; 2:554-574. DOI: 10.3390/polym2040554
- [44] O. Faruk, A.K. Bledzki, H. Fink, M. Sain. Biocomposites reinforced with natural fibers: 2000-2011. *Progress in Polymer Science* 2012; 37:1552-1596. DOI: 10.1016/j.progpolymsci.2012.04.003
- [45] T. Nishino, K. Hirao, M. Kotera, K. Nakamae, H. Inagaki. Kenaf reinforced biodegradable composites. *Composites Science and Technology* 2003; 63:1281-1286. DOI: 10.1016/S0266-3538(03)00099-X
- [46] G. Bogoeva-Gaceva, M. Avella, M. Malinconico, A. Buzarovska, A. Grozdanov, G. Gentile, M.E. Errico. Natural fiber eco-composites. *Polymer Composites* 2007; 28:98-107. DOI: 10.1002/pc.20270
- [47] A.A. Yussuf, I. Massoumi, A. Hassan. Comparison of polylactic acid/kenaf and polylactic acid/rise husk composites: The influence of the natural fibers on the mechanical, thermal and biodegradability properties. *Journal of Polymers and the Environment* 2010; 18:422-429. DOI: 10.1007/s10924-010-0185-0

- [48] W. Letian, T. Zhaohui, O. Lonnie, Q.C. Ingram, M. Siobhan. Green composites of poly(lactic acid) and sugarcane bagasse residues from bio-refinery processes. *Journal of Polymers and the Environment* 2013; 21:780-788.
DOI: 10.1007/s10924-013-0601-3
- [49] M. Wollerdorfer, H. Bader. Influence of natural fibres on the mechanical properties of biodegradable polymers. *Industrial Crops and Products* 1998; 8:105-112.
DOI: 10.1016/S0928-66
- [50] M.U. Wahit, N.I. Akos, W.A. Laftah. Influence of natural fibers on the mechanical properties and biodegradation of poly(lactic acid) and poly(ϵ -caprolactone) composites: A review. *Polymer Composites* 2012; 33:1045-1053.
DOI: 10.1002/pc.22249
- [51] H. Liu, J. Zhang. Research progress in toughening modification of poly(lactic acid). *Polymer Physics* 2011; 49:1051-1083.
DOI: 10.1002/polb.22283
- [52] N. Reddy, D. Nama, Y. Yang. Polylactic acid/polypropylene polyblends fibers for better resistance to degradation. *Polymer Degradation and Stability* 2008; 93:233-241.
DOI: 10.1016/j.polymdegradstab.2007.09.005
- [53] X. Liu, L.Lei, J. Hou, M. Tang, S. Guo, Z. Wang, K. Chen. Evaluation of two polymeric blends (EVA/PLA and EVA/PEG) as coating film materials for paclitaxel-eluting stent application. *Journal of Material Science* 2011; 22:327-337.
DOI: 10.1007/s10856-010-4213-3
- [54] I. Moura, G. Botelho, A.V. Machado. Characterization of EVA/PLA blends when exposed to different environment. *Journal of Polymers and the Environment* 2014; 22:148-157.
DOI: 10.1007/s10924-013-0614-y
- [55] P. Ma, X. Cai, Y. Zhang, S. Wang, W. Dong, M. Chen, P.J. Lemstra. In-situ compatibilization of poly(lactic acid) and poly(butylene adipate-co-terephthalate) blends by using dicumyl peroxide as a free-radical initiator. *Polymer Degradation and Stability* 2014; 102:145-151.
DOI: 10.1016/j.polymdegradstab.2014.01.025

- [56] A. Benyahia, A. Merrouche, Z.E.A. Rahmouni, M. Rokbi, W. Serge, Z. Kouadri. Study of the alkali treatment effect on the mechanical behavior of the composites unsaturated polyester-alfa fiber. *Mechanics and Industry* 2014; 15:69-73.
DOI: 10.1051/meca/2013082
- [57] S. Kalia, A. Dufresne, B.M. Cherian, B.S. Kaith, L. Avèrous, J. Njuguna, E. Nassiopoulou. Cellulose-based bio-and nanocomposites: A review. *International Journal of Polymer Science* 2011; 2011:1-35.
DOI: 10.1155/2011/837875
- [58] G. Jayamol, M.S. Sreekala, S. Thomas. A review on interface modification and characterization of natural fibre reinforced plastic composites. *Polymer Engineering and Science* 2001; 41:1471-1485.
DOI: 10.1002/pen.10846
- [59] X. Li, L.G. Tabil, S. Panigrahi. Chemical treatments of natural fibre for use in natural fibre-reinforced composites. *Journal of Polymers and the Environment* 2007; 15:25-33.
DOI: 10.1007/s10924-006-0042-3
- [60] F.P. La Mantia, M. Morreale. Green composites: A brief review. *Composites: Part A* 2011, 42:579-588.
DOI:10.1016/j.compositesa.2011.01.017
- [61] W. Liu, A.K. Mohanty, P.A. L.T. Drzal, M. Misra. Influence of fiber surface treatment on properties of Indian grass fiber reinforced soy protein based biocomposites. *Polymer* 2004; 45:7589-7596.
DOI: 10.1016/j.polymer.2004.09.009
- [62] A.M.M. Edeerozey, H. Md Akil, A.B. Azhar, M.I.Z. Ariffin. Chemical modification of kenaf fibres. *Materials Letters* 2007; 61:2023–2025.
DOI: 10.1016/j.matlet.2006.08.006
- [63] W.L. Lai, M. Mariatti, S.M. Jani. The properties of woven kenaf and betel palm(*Areca catechu*) reinforced unsaturated polyester composites. *Polymer-Plastics Technology and Engineering* 2008; 47:1193-1199.
DOI: 10.1080/03602550802392035
- [64] N.A. Ibrahim, K.A. Hadithon, K. Abdan. Effect of fibre treatment on mechanical properties of kenaf-Ecoflex composites. *Journal of Reinforced Plastics and Composites*

2010; 29:2921-2198.

DOI: 10.1177/0731684409347592

- [65] C.R. Soccol, L.P.D. Vandenberghe, A.B.P. Medeiros, S.G. Karp, M. Buckeridge, L.P. Ramos, A.P. Pitarelo, V. Ferreira-Leitao, L.M.F. Gottschalk, M.A. Ferrara, E.P.D. Bon, L.M.P. de Moraes, J.D. Araujo. Bioethanol from lignocelluloses: Status and perspectives in Brazil. *Bioresource Technology* 2010; 101:4820-4825.
DOI: 10.1016/j.biortech.2009.11.067
- [66] C. Driemeier, M.M. Oliveira, F.M. Mendes, E.O. Gomez. Characterization of sugarcane bagasse powders. *Powder Technology* 2011; 214:111-116.
DOI: 10.1016/j.powtec.2011.-7.043
- [67] S. Ata, F.H. Wattoo, M. Ahmed, M.H.S. Wattoo, S.A. Tirmizi, A. Wadood. A method optimization study for atomic absorption spectrophotometric determination of total zinc in insulin using direct aspiration technique. *Alexandria Journal of Medicine* 2015; 51:19-23.
DOI: 10.1016/j.ajme.2014.03.004
- [68] N. Reddy, Y. Yang. Biofibres from agricultural byproducts for industrial applications. *Trends in Biotechnology* 2005; 23:22-27.
DOI: 10.1016/j.tibtech.2004.11.002
- [69] A.K. Mohanty, M. Misra, G. Hinrichsen. Biofibres, biodegradable polymers and biocomposites: An overview. *Macromolecular Materials and Engineering* 2000; 276/277:1-24.
DOI: 10.1002/(SICI)1439-2054(20000301)276
- [70] M.M. Kabir, H. Wang, K.T. Lau, F. Cardona. Chemical treatments on plant-based natural fibre reinforced polymer composites: An overview. *Composites: Part B* 2012; 43:2883-2892.
DOI: 10.1016/j.compositesb.2012.04.053
- [71] A.K. Bledzki, J. Gassan. Composites reinforced with cellulose based fibres. *Progress in Polymer Science* 1999; 24:221-274.
DOI: 10.1016/S0079-6700(98)00018-5
- [72] V.K. Thakur, M.K. Thakur. Processing and characterization of natural cellulose fibers/thermoset polymer composites. *Carbohydrate Polymers* 2014; 109:102-117.

DOI: 10.1016/j.carpol.2014.03.039

- [73] J.L. Guimarães, E. Frollini, C.G. da Silva, F. Wypych, K.G. Satyanarayana. Characterization of banana, sugarcane bagasse and sponge gourd fibers of Brazil. *Industrial Crops and Products* 2009; 30:407-415.
DOI: 10.1016/j.indcrop.2009.07.013
- [74] K.M.M. Rao, K.M. Rao. Extraction and tensile properties of natural fibers: Vakka, date and bamboo. *Composite Structures* 2007; 77:288-295.
DOI: 10.1016/j.compstruct.2005.07.023
- [75] A.G. Kulkarni, K.G. Satyanarayana, P.K. Rohatgi, K. Vijayan. Mechanical properties of banana fiber (*Musa sapientum*). *Journal of Materials Science* 1983; 18:2292-2296.
DOI: 10.1007/BF00541832
- [76] L. Canilha, A.K. Chandel, T.S.S. Milessi, F.A.F. Antunes, W.L.C. Freitas, M.G.A. Felipe, S.S. Silva. Bioconversion of sugarcane biomass into ethanol: An overview about composition, pretreatment methods, detoxification of hydrolysates, enzymatic saccharification, and ethanol fermentation. *Journal of Biomedicine and Biotechnology* 2012; 2012:1-15.
DOI:10.1155/2012/989572
- [77] L. Canilha, R. de Cássia Lacerda Brambilla Rodrigues, F.A.F. Antunes, A.K. Chandel, T.S. dos Santos Milessi, M. das Graças Almeida Felipe, S.S. da Silva. Bioconversion of hemicellulose from sugarcane biomass into sustainable products. In: *Sustainable Degradation of Lignocellulosic Biomass-Techniques, Applications and Commercialization* (edited by A.K Chandel and S.S. da Silva). INTECH Open Science (2013).
DOI: 10.5772/53832
- [78] I. Ullah, R. Nadeem, M. Iqbal, Q. Manzoor. Biosorption of chromium onto native and immobilized sugarcane bagasse waste biomass. *Ecological Engineering* 2013; 60:99-107.
DOI: 10.1016/j.ecoleng.2013.07.028
- [79] F. Peng, J. Ren, F. Xu, J. Bian, P Peng, R. Sun. Comparative study of hemicelluloses obtained by graded ethanol precipitation from sugarcane bagasse. *Journal of Agricultural and Food Chemistry* 2009; 57:6305-6317.
DOI: 10.1021/jf900986b

- [80] A. Pandey, C.R. Soccol, P. Nigam, V.T. Soccol. Biotechnological potential of agro-industrial residues. I: sugarcane bagasse. *Bioresource Technology* 2000; 74: 69-80.
DOI: 10.1016/S0960-8524(99)00142-X
- [81] S.E. Jacobsen, C.E. Wyman. Xylose monomer and oligomer yields for uncatalyzed hydrolysis of sugarcane bagasse hemicellulose at varying solids concentration. *Industrial Engineering of Chemical Resource* 2002; 41:1454-1461.
DOI: 10.1021/ie001025
- [82] Y. Lee, C. Chung, D.F. Day. Sugarcane bagasse oxidation using a combination of hypochlorite and peroxide. *Bioresource Technology* 2009; 100:935-941.
DOI:10.1016/j.biortech.2008.06.043
- [83] G.J.M. Rocha, V.M. Nascimento, A.R. Gonçalves, V.F.N. Silva, C. Martín. Influence of mixed sugarcane bagasse samples evaluated by elemental and physical-chemical composition. *Industrial Crops and Products* 2015; 64:52-58.
DOI: 10.1016/j.indcrop.2014.11.003
- [84] T.E. Motaung, R.D. Anandjiwala. Effect of alkali and acid treatment on thermal degradation kinetics of sugarcane bagasse. *Industrial Crops and Products* 2015; 74:472-477
DOI: 10.1016/j.indcrop.2015.05.062
- [85] A. Ounas, A. Aboukhas, K. El harfi, A. Bacaoui, A. Yaacoubi. Pyrolysis of olive residue and sugarcane bagasse: Non-isothermal thermogravimetric kinetic analysis. *Bioresource Technology* 2011; 102:11234-11238.
DOI: 10.1016/j.biortech.2011.09.010
- [86] C.G. Mothé, I.C. de Miranda. Study of kinetic parameters of thermal decomposition of bagasse and sugarcane straw using Friedman and Ozawa-Flynn-Wall isoconversional methods. *Journal of Thermal Analysis and Calorimetry* 2013; 113:497-505.
DOI: 10.1007/s10973-013-3163-7
- [87] M. Garcia-Pérez, A. Chaala, J. Yong, C. Roy. Co-pyrolysis of sugarcane bagasse with petroleum residue. Part I: Thermogravimetric analysis. *Fuel* 2001; 80:1245-1258.
DOI: 10.1016/S0016-2361(00)00215-5
- [88] J.O. Agunsoye, V.S. Aigbodion. Bagasse filled recycled polyethylene bio-composites: Morphology and mechanical properties study. *Results in Physics* 2013; 3:187-194.

DOI: 10.1016/j.rinp.2013.09.003

- [89] S.I. Hossain, M. Hasan, Md.N. Hasan, A. Hassan. Effect of chemical treatment on physical, mechanical and thermal properties of ladies finger natural fiber. *Advances in Materials Science and Engineering* 2013; 2013:1-6.
- [90] S.S. Mir, S.M.N. Hasan, Md,J. Hossain, M. Hasan. Chemical modification effect on the mechanical properties of coir fiber. *Engineering Journal* 2012; 16:73-83.
DOI: 10.4186/ej.2012.16.2.73
- [91] L.Y. Mwaikambo, M.P. Ansell. Chemical modification of hemp, sisal, jute, and kapok fibers by alkalization. *Journal of Applied Polymer Science* 2002; 84:2222- 2234.
DOI: 10.1002/app.10460
- [92] E. Jayamani, S. Hamdan, S.K. Heng, Md R. Rahman, M.K. Bakri, A. Kakar. The effect of natural fibres mercerization on natural fibres/polypropylene composites: A study of thermal stability, morphology and infrared spectrum. *Australian Journal of Basic and Applied Sciences* 2014; 8:332-340.
- [93] H. Gao, Y. Xie, R. Ou, Q. Wang. Grafting effect of polypropylene/polyethylene blends with maleic anhydride on the properties of the resulting wood-plastic composites. *Composites: Part A* 2012; 43:150-157.
DOI: 10.1016/j.compositesa.2011.10.001
- [94] P.N. Khanam, M.A. AlMaadeed. Improvement of ternary recycled polymer reinforced with date palm fibre. *Materials and Design* 2014; 60:532-539.
DOI: 10.1016/j.matdes.2014.04.033
- [95] N.I. Akos, M.U. Wahit, R. Mohamed, A.A. Yussuf. Preparation, characterization, and mechanical properties of poly(ϵ -caprolactone)/polylactic acid blend composites. *Polymer Composites* 2013; 34:763-768.
DOI: 10.1002/pc.22488
- [96] A.I. Khalf, A.A. Ward. Use of rice husk as potential filler in styrene butadiene rubber/linear low density polyethylene blends in the presence of maleic anhydride. *Materials and Design* 2010; 31:2414-2421.
DOI: 10.1016/j.matdes.2009.11.056
- [97] C. Clemons. Elastomer modified polypropylene-polyethylene blends as matrices for wood flour-plastic composites. *Composites: Part A* 2010; 41:1559-1569.

- DOI: 10.1016/j.compositesa.2010.07.002
- [98] Y. Lei, Q. Wu. High density polyethylene and poly(ethylene terephthalate) *in situ* sub-micro-fibril blends as a matrix for wood plastic composites. *Composites: Part A* 2012; 43:73-78.
DOI: 10.1016/j.compositesa.2011.09.01
- [99] N. Saba, M.T. Paridah, M. Jawaid. Mechanical properties of kenaf fibre reinforced polymer composite: A review. *Construction and Building Materials* 2015, 76:87-96.
DOI: 10.1016/j.conbuildmat.2014.11.043
- [100] A. Espert, F. Vilaplana, S. Karlsson, Comparison of water absorption in natural cellulosic fibres from wood and one-year crops in polypropylene composites and its influence on their mechanical properties. *Composites: Part A* 2004; 35:1267-1276.
DOI:10.1016/j.compositesa.2004.04.004
- [101] H.N. Dhakal, Z.Y. Zhang, M.O.W. Richardson. Effect of water absorption on the mechanical properties of hemp fibre reinforced unsaturated polyester composites. *Composites Science and Technology* 2007; 67:1674-1683.
DOI:10.1016/j.compscitech.2006.06.019
- [102] S.K. Najafi, M. Tajvidi, M. Chaharmahli. Long-term water uptake behavior of lignocellulosic-high density polyethylene composites. *Journal of Applied Polymer Science* 2006; 102:3907-3911.
DOI 10.1002/app.24172
- [103] H.S. Yang, H.J. Kim, H.J. Park, B.J. Lee, T.S. Hwang. Water absorption behavior mechanical properties of lignocellulosic filler-polyolefin bio-composites. *Composite Structures* 2006; 72:429-437.
DOI:10.1016/j.compstruct.2005.01.013
- [104] D.G. Dikobe, A.S. Luyt. Effect of poly(ethylene-co-glycidyl methacrylate) compatibilizer content on the morphology and physical properties of ethylene vinyl acetate-wood fiber composites. *Journal of Applied Polymer Science* 2007; 104:3206-3213.
DOI: 10.1002/app.26080
- [105] V.A. Alvarez, A. Vázquez. Effect of water sorption on the flexural properties of a fully biodegradable composite. *Journal of Composite Materials* 2004; 38:1165-1182.
DOI: 10.1177/0021998304042082

- [106] M. Tajvidi, S.K Najafi, N. Moteei. Long-term water uptake behaviour of natural fiber/polypropylene composites. *Journal of Applied Polymer Science* 2006; 99:2199-2203. DOI: 10.1002/app.21892
- [107] D. Sud, G. Mahajan, M.P. Kaur. Agricultural waste material as potential adsorbent for sequestering heavy metal ions from aqueous solutions: A review. *Bioresource Technology* 2008; 99:6017-6027. DOI: 10.1016/j.biortech.2007.11.064
- [108] B. Singha, S.Kr. Das. Adsorptive removal of Cu(II) from aqueous solution and industrial effluent using natural/agricultural wastes. *Colloids and Surfaces B: Biointerfaces* 2013; 107:97-106. DOI: 10.1016/j.colsurfb.2013.01.060
- [109] P.M. Shukla, S. R. Shukla. Biosorption of Cu(II), Pb(II), Ni(II), and Fe(II) on alkali treated coir fibers. *Separation Science and Technology* 2013;48:421-428. DOI: 10.1080/01496395.2012.691933
- [110] S.M.A. Andrabi. Sawdust of lam tree (*Cordia africana*) as a low-cost, sustainable and easily available adsorbent for the removal of toxic metals like Pb(II) and Ni(II) from aqueous solution. *European Journal of Wood and Wood Products* 2011; 69:75-83. DOI: 10.1007/s00107-009-0398-x
- [111] C. Duan, N. Zhao, X. Yu, X. Zhang, J. Xu. Chemically modified kapok fiber for fast adsorption of Pb²⁺, Cd²⁺, Cu²⁺ from aqueous solution. *Cellulose* 2013; 20:849-860. DOI: 10.1007/s10570-013-9875-9
- [112] G. Akkaya, F. Güzel. Bioremoval and recovery of Cu(II) and Pb(II) from aqueous solution by a novel biosorbent watermelon (*Citrullus lanatus*) seed hulls: Kinetic study, equilibrium isotherm, SEM and FTIR analysis. *Desalination and Water Treatment* 2013; 51:7311-7322. DOI: 10.1080/19443994.2013.815685
- [113] B.M.W.P.K. Amarasinghe, R.A. Williams. Tea waste as a low cost adsorbent for the removal of Cu and Pb from wastewater. *Chemical Engineering Journal* 2007; 132:299-309. DOI: 10.1016/j.cej.2007.01.016
- [114] W.P. Putra, A. Kamari, S.N.M. Yusoff, C.F. Ishak, A. Mohamed, N. Hashim, I.M. Isa. Biosorption of Cu(II), Pb(II) and Zn(II) ions from aqueous solutions using selected waste

- materials: Adsorption and characterisation studies. *Journal of Encapsulation and Adsorption Sciences* 2014; 4:25-35.
DOI: 10.4236/jeas.2014.41004
- [115] A. Ahmada, M. Rafatullahb, O. Sulaimanb, M.H. Ibrahima, Y.Y. Chiia, B.M. Siddique. Removal of Cu(II) and Pb(II) ions from aqueous solutions by adsorption on sawdust of Meranti wood. *Desalination* 2009; 247:636-646.
DOI: 10.1016/j.desal.2009.01.007
- [116] X. Tang, Q. Zhang, Z. Liu, K. Pan, Y. Dong, Y. Li. Removal of Cu(II) by loofah fibers as a natural and low-cost adsorbent from aqueous solutions. *Journal of Molecular Liquids* 2014; 191:73-78.
DOI: 10.1016/j.molliq.2013.11.034
- [117] S. Lin, Z. Song, G. Che, A. Ren, P. Li , C. Liu , J. Zhang. Adsorption behaviour of metal-organic frameworks for methylene blue from aqueous solution. *Microporous and Mesoporous Materials* 2014; 193:27-34.
DOI: 10.1016/j.micromeso.2014.03.004
- [118] P.L. Homagai, K.N. Ghimire, K. Inoue. Adsorption behavior of heavy metals onto chemically modified sugarcane bagasse. *Bioresource Technology* 2010;101:2067-2069.
DOI: 10.1016/j.biortech.2009.11.073
- [119] L.V.A. Gurgel, R.P. Freitas, L.F. Gil. Adsorption of Cu(II), Cd(II), and Pb(II) from aqueous single metal solutions by sugarcane bagasse and mercerized sugarcane bagasse chemically modified with succinic anhydride. *Carbohydrate Polymers* 2008; 74:922-929.
DOI: 10.1016/j.carbpol.2008.05.023
- [120] I. Ullah, R. Nadeem, M. Iqbal, Q. Manzoor. Biosorption of chromium onto native and immobilized sugarcane bagasse waste biomass. *Ecological Engineering* 2013; 60:99-107.
DOI: 10.1016/j.ecoleng.2013.07.028
- [121] O.E.A. Salam, N.A. Reiad, M.M. ElShafei. A study of the removal characteristics of heavy metals from wastewater by low-cost adsorbents. *Journal of Advanced Research* 2011; 2:297-303.
DOI: 10.1016/j.jare.2011.01.008

CHAPTER 2

Materials and methods

2.1 Materials

Poly(L-lactic acid) (PLLA) was supplied by Toyota Motor Co., Japan. It has a molecular weight of 557 000 g mol⁻¹, viscosity of 5340 Pa s at 180 °C, T_m of 170-180 °C, T_g of 50-60 °C, and a density of 1.248 g cm⁻³.

The ethylene vinyl acetate copolymer (EVA-460) was manufactured and supplied in granule form by DuPont Packaging & Industrial Polymers. EVA-460 contains 18% by weight of vinyl acetate (VA) with a butylated hydroxy toluene (BHT) antioxidant thermal stabilizer. It has a melt flow index (MFI) of 2.5 g/10 min (190 °C/2.16 kg, ASTM D1238/ISO 11330), T_m of 88 °C, Vicat softening point of 64 °C, and a density of 0.941 g cm⁻³.

Sugarcane bagasse (SCB) was supplied by a farm in Craddock near Port Elizabeth, South Africa.

Table 2.1 Composition of SCB

Sample	Lignin / %	Cellulose / %	Hemicellulose / %
Sugarcane bagasse (SCB)	2.8 ± 1.3	48.8 ± 0.1	47.2 ± 0.8

Dicumyl peroxide was supplied by Sigma-Aldrich, Krugersdorp, South Africa as a white crystalline powder with an assay of 99%. It was used as a free radical initiator and has a melting point of 39 °C and a molar mass of 270 g mol⁻¹.

2.2 Methods

2.2.1 Pre-treatment of SCB

SCB was washed extensively with boiling distilled water to remove any excess sugar contained within and to prevent fungal growth. SCB was air dried for 24 hours followed by oven drying for another 24 hours at 80 °C to remove moisture. It was then soaked in 10% NaOH for 1 hour and washed several times with distilled water to remove the remaining alkali from the fibre. SCB was then immersed in 0.25 M acetic acid to neutralize it, and litmus paper was used to check the neutrality of the SCB. Distilled water was used to wash the remaining acetic acid. A vacuum filter was used to filter SCB, and it was air dried for 24 hours followed by oven drying for 24 hours at 80 °C. After drying, it was crushed with an analytical mill to obtain a fine powder which was sieved with a 425 µm sieve. The reasons for applying alkaline treatment on the fibre surface were: (i) to distribute the hydrogen bonds in the network structure, thereby increasing the surface roughness, (ii) to remove a certain amount of lignin, wax and natural oils covering the external surface of the fibre wall, and (iii) to depolymerise and expose the short length crystallites [1].

2.2.2 Sample preparation

The sample ratios (quantities) of the biocomposites are shown in Table 2.1. PLA and EVA were oven dried at 60 °C for 24 hours to remove any moisture trapped within the granules. All the samples were prepared by melt mixing using a Brabender Plastograph with a 50 mL internal mixer. The samples were prepared at 180 °C, at a speed of 60 rpm for 15 min. A temperature of 180 °C was chosen to fully melt the crystals, and at the same time avoiding sample degradation and high torque levels in the Brabender [2]. PLA and EVA were physically premixed and fed into the heated mixer. They were allowed to mix for 2 min, after which SCB was introduced and the mixing continued for another 13 min. 0.1 phr DCP was added to the mixture (PLA/EVA/SCB) one minute before the end of the mixing time. DCP was used to improve adhesion between PLA and EVA. PLA/EVA/SCB samples were then melt pressed at 180 °C for 10 min under 50 kPa using a hydraulic melt press. They were cooled for 5 min between steel bars and cut for different characterizations.

Table 2.2 Sample compositions used in this study

PLA/EVA/SCB(w/w)	PLA/EVA/SCB(w/w)	PLA/EVA/SCB(w/w)
50/50/0	70/30/0	90/10/0
47.5/47.5/5	66.5/28.5/5	85.5/9.5/5
45/45/10	63/27/10	81/9/10
42.5/42.5/15	59.5/25.5/15	76.5/8.5/15
40/40/20	56/24/20	72/8/20
35/35/30	49/21/30	63/7/30

2.3 Sample analysis

To determine the viscosity of the polymers, a melt flow index of the two polymers in the blend was determined using a CEAST Melt Flow Junior. Ten samples each of both polymers were analysed at 190 °C. The amount of samples which flowed through the die over a period of 10 minute under 2.16 Kg weight was determined in each case.

Contact angle tests were performed at room temperature on surface energy evaluation system. Contact angles of two test liquids (distilled water H₂O and diiodomethane CH₂I₂) were measured by depositing a drop on the sample and the values were estimated as the tangent normal to the drop at the intersection between the sessile drop and the surface. Images were taken within 30 seconds of the drop deposition to avoid solvent evaporation. The reported contact angle values are the average of at least five measurements at different spots of the surface of the sample. Surface energies of SCB were obtained from the literature [3]. Distilled water (H₂O) and diiodomethane (CH₂I₂) were used as polar and non-polar solvents, respectively. The literature values of their surface energies are: (H₂O; $\gamma^p = 34.2 \text{ mJ m}^{-2}$; CH₂I₂; $\gamma^d = 17.8 \text{ mJ m}^{-2}$). The contact angle, total surface energy, as well as their dispersive and polar surface components, were calculated using Owens-Wendth method (Equations 2.1 and 2.2) [4-7].

$$\gamma_s = \gamma_s^d + \gamma_s^p \quad (2.1)$$

$$\gamma_1(1 + \cos\theta) = 2\sqrt{\gamma_s^d \cdot \gamma_l^d} + 2\sqrt{\gamma_s^p \cdot \gamma_l^p} \quad (2.2)$$

where θ is the contact angle, γ is the surface energy, the subscripts 's' and 'l' indicate solid and liquid respectively, while the superscripts 'd' and 'p' indicate the dispersive and polar components, respectively. The interfacial tensions between the components in a blend were calculated from contact angle measurement results using the geometric mean equation (Equation 2.3) [4-7].

$$\gamma_{12} = \gamma_1 + \gamma_2 - 2(\sqrt{\gamma_1^d \cdot \gamma_2^d} + \sqrt{\gamma_1^p \cdot \gamma_2^p}) \quad (2.3)$$

where γ_{12} = interfacial tension between components 1 and 2 in the blend, γ_1 and γ_2 are the total surface energies of components 1 and 2, γ_1^d and γ_2^d are the dispersive surface energies of components 1 and 2, and γ_1^p and γ_2^p are the polar surface energies of the components 1 and 2 in the composites. The wetting coefficient was calculated using the interfacial tensions of the PLA/EVA, PLA/SCB and EVA/SCB from Young's equation (Equation 2.4) [4-8].

$$\omega_a = \frac{\gamma_{PLA/SCB} - \gamma_{EVA/SCB}}{\gamma_{PLA/EVA}} \quad (2.4)$$

where $\gamma_{PLA/SCB}$ is the interfacial tension between PLA and SCB, $\gamma_{EVA/SCB}$ is the interfacial tension between EVA and PLA, and $\gamma_{PLA/EVA}$ is the interfacial tension between PLA and EVA. If $\omega_a < -1$, the particles are predicted to be located in polymer B in this case (EVA). If $\omega_a > 1$ they are dispersed in polymer A (PLA), and if the value of ω_a is between -1 and 1, the particles are likely to disperse on the interface of the two polymers in the blend.

An optical microscope (CETI-Topic B, Belgium) was used to examine the dispersion of the fibres in the polymer matrices, as well as the morphologies of the composite samples. The micrographs of the biocomposites were taken at 4x (SP 4x/0.10/160/-) magnification.

The morphologies of the blends and the PLA/EVA/SCB biocomposites were investigated by a TESCAN VEGA 3 scanning electron microscope (SEM). All the blends and biocomposite samples were fractured under liquid nitrogen to avoid any disturbance to the molecular structure. They

were coated with gold to ensure that the charge deposited on the sample surface by the electron beam was able to leak away to the earth [9,10], and examined at an acceleration voltage of 15 kV.

Attenuated total reflectance Fourier-transform infrared spectroscopy (ATR-FTIR) spectra of the neat materials and the PLA/EVA/SCB samples were obtained using a Perkin Elmer Spectrum 100 FTIR spectrometer. The samples were analysed over a range of 650-4000 cm^{-1} with a resolution of 4 cm^{-1} . All the spectra were averaged over 16 scans.

A Ceast Impactor II was used to investigate the impact properties of the blends and composites, in order to establish whether SCB gave rise to improved impact properties. The samples were rectangular with a width of 10 mm, a thickness of 3 mm and length of 83 mm, and they were V-notched (3 mm deep) edgewise. The pendulum hammer was situated at an angle of 50° from the release spot and the samples were tested at an ambient temperature of 24 °C. Five samples of each composition were tested and the average and standard deviation values are presented.

Samples (2 mm x 10 mm x 40 mm) of 50/50 and 70/30 w/w PLA/EVA, as well as their composites containing respectively 15, 20 and 30% SCB, were first dried at 30 °C in an oven for 24 hours to ensure that they were completely dry. The weights of the samples were recorded before they were immersed in distilled water at various time intervals. At each interval, the samples were removed from the distilled water and blot dried with a paper towel before recording their masses after insertion in water. This procedure was repeated until there was no further increase in the weight of the samples. All the measurements were done in triplicate, and the mean and standard deviation values were calculated. The percentage water absorption was calculated using Equation 2.5.

$$\%W = \frac{W_t - W_i}{W_i} \times 100 \quad (2.5)$$

where W is the total water absorbed, W_t is the final weight of the sample after a certain time t of water immersion, and W_i is the initial sample mass.

A flame atomic absorption spectrometer (GBC 909AA) was used for the adsorption analysis of the samples. The adsorption experiments were done by measuring 50 mL of the metal solutions into a 100 mL beaker and adding 2 g of the previously prepared composites (cut into small strips of about 2 mm x 40 mm x 10mm) into the metal solution. The beaker containing the adsorbent and the metal solution was placed on a magnetic stirrer and stirred at 150 rpm at a room temperature of 25.6 °C for a period of 5 hours to ensure equilibrium. The suspension was filtered using Whatman filter paper. The first 5 mL of each filtrate was thrown away because filter paper is cellulose and can absorb some metal ions. The atomic absorption spectrophotometer was used to analyse the concentrations of metal ions present in the filtrate. The amount of concentration of the metal ions adsorbed C_a by the adsorbent was evaluated using Equation 2.6.

$$C_a = C_o - C_e \quad (2.6)$$

where C_o and C_e are the initial and final concentrations (mg L^{-1}) of the heavy metals present in the metal solution before and after adsorption for a time t . C_e represents the concentrations (mg L^{-1}) of heavy metal ions in the metal solution when equilibrium was attained. The percentage of metal ions removed was obtained from Equation 2.7.

$$R(\%) = \frac{C_o - C_e}{C_o} \times 100 \quad (2.7)$$

where R is the removal efficiency of the adsorbent.

Effect of contact time: The effect of contact time on the removal of the metal ions was studied for a period of 5 hours. 2 g of the adsorbents (PLA/EVA/SCB biocomposites) were added to different beakers containing 50 mL of metal solutions at a pH of 5. The beaker was closed with a sapphire, placed in a magnetic stirrer, and agitated at 150 rpm for each of the different contact times chosen (30 min, 1 hr, 3 hr, and 5 hr). The content of each beaker was filtered and analysed after each agitation time.

Effect of pH: The effect of pH on the adsorption of the metal ions was studied over a pH range of 3 to 9. For this particular study, 50 mL of metal solution was measured into different 100 mL beakers and 2 g of the adsorbent, being the optimum adsorbent from the previous experiment, was added and agitated at 150 rpm for 5 hours. The pH was adjusted using 1 M HCl and 1 M NaOH for each of the chosen pH values (3, 5, 7 and 9). Whatman filter paper was used to filter the mixture and the filtrate analysed to determine the concentrations of metal ions.

Effect of initial concentration: The initial concentration of the metal solution was varied from 100 to 400 ppm. 2 g of the adsorbents was added to different beakers containing 50 mL of metal solution, closed and agitated in a magnetic stirrer for a period of 5 hours at room temperature. The content of each flask was then filtered and analysed after the agitation time.

Thermogravimetric analysis in a Perkin-Elmer STA6000 thermogravimetric analyser was used to study the thermal stabilities of the neat PLA, EVA, and SCB, and the biocomposite samples. 20-25 mg samples were heated under a flowing nitrogen atmosphere (20 mL min⁻¹) from 30 °C to 550 °C at a heating rate of 10 °C min⁻¹, and the corresponding mass loss was recorded.

Differential scanning calorimetry (DSC) analyses were performed in a Perkin-Elmer Pyris-1 differential scanning calorimeter DSC. Samples of 5-10 mg were sealed in aluminium pans and heated under nitrogen flow (20 mL min⁻¹) from -10 to 195 °C at a heating rate of 10 °C min⁻¹, and kept at this temperature for 1 min to erase the thermal history. The samples were then cooled and re-heated under the same conditions. At least three separate measurements were made to ensure reproducibility. The glass transition, cold crystallization, and melting temperatures, as well as the melting and cold crystallization enthalpies, of the samples were determined from the second heating runs as the average of three measurements. The degree of crystallinity was calculated using the total enthalpy method, according to Equation 2.8.

$$X_c = \frac{\Delta H_m}{\Delta H_m^o} \times 100 \quad (2.8)$$

where X_c is the degree of crystallinity, ΔH_m is the specific enthalpy of melting of a polymer, and ΔH_m^0 is the specific enthalpy of melting for 100% crystalline PLA and EVA. Values of 93.0 J g^{-1} and 272 J g^{-1} for PLA and EVA were used respectively in the calculations.

2.4 References

- [1] E. Jayamani, S. Hamdan, S.K. Heng, Md. R. Rahman, M.K. Bakri, A. Kakar. The effect of natural fibres mercerization on natural fibres/polypropylene composites: A study of thermal stability, morphology and infrared spectrum. *Australian Journal of Basic and Applied Sciences* 2014; 8:332-340.
- [2] S.M.A. Andrabi. Sawdust of lam tree (*Cordia africana*) as a low-cost, sustainable and easily available adsorbent for the removal of toxic metals like Pb(II) and Ni(II) from aqueous solution. *European Journal of Wood and Wood Products* 2011; 69:75-83.
DOI: 10.1007/s00107-009-0398-x
- [3] D. Pasquini, M.N. Belgacem, A. Gandini, Antonio A.S. Curvelo. Surface esterification of cellulose fibers: Characterization by DRIFT and contact angle measurements. *Journal of Colloid and Interface Science* 2006; 295:79-83.
DOI: 10.1016/j.jcis.2005.07.074
- [4] D. Wu, D. Lin, J. Zhang, W. Zhou, Ming Zhang, Y. Zhang, D. Wang, B. Lin. Selective localization of nanofillers: Effect on morphology and crystallization of PLA/PCL blends. *Macromolecular Chemistry and Physics* 2011; 212:613-626.
DOI: 10.1002/macp.201000579
- [5] X. Wang, K. Xu, X. Xu, S. Park, S. Kim. Selective particle distribution and mechanical properties of nano-CaCO₃/ethylene-propylene-diene terpolymer/polypropylene composites with high content of nano-CaCO₃. *Journal of Applied Polymer Science* 2009; 113: 2485-2491.
DOI: 10.1002/app
- [6] H. Xiu, H.W. Bai, C.M. Huang, C.L. Xu, X.Y. Li, Q. Fu. Selective localization of titanium dioxide nanoparticles at the interface and its effect on the impact toughness of poly(L-lactide)/poly(ether)urethane blends. *Express Polymer Letters* 2013; 7:261-271.
DOI: 10.3144/expresspolymlett.2013.24

- [7] F. Fenouillot, P. Cassagnau, J.C. Majesté. Uneven distribution of nanoparticles in immiscible fluids: Morphology development in polymer blends. *Polymer* 2009; 50:1333-1350
DOI: 10.1016/j.polymer.2008.12.092
- [8] B. Zhao, R.W. Fu, M.Q. Zhang, H. Yang, M.Z. Rong, Q. Zheng. Effect of soft segments of waterborne polyurethane on organic vapour sensitivity of carbon black filled waterborne polyurethane composites. *Polymer Journal* 2006; 38:799-806.
DOI: 10.1295/polmj.PJ2005202
- [9] C.E. Carraher Jr. *Carraher's Polymer Chemistry* 8th Edition. CRC Press Taylor & Francis Group: Boca Raton (2011).
- [10] B.J. Hunt, M.I. James. *Polymer Characterisation*. Blackie Academic & Professional: London (1993).

CHAPTER 3

Results and discussion

3.1 Selective dispersion of the SCB in the polymer blend

The selective localization of a filler is important to the morphology design and property control of an immiscible polymer blend system. This selective localization behaviour mainly results from large differences in the affinity between the filler and the two matrix components. Thermodynamic (surface properties) and kinetic (viscosity) effects are two factors involved in determining the selective localization of filler in a two-phase polymer blend system. The filler will selectively locate itself in order to balance viscoelastic properties of the polymer, reduce interfacial tension and also reduce the surface energy of the polymer in the system. This may improve the interfacial interaction between the two polymers in the system if the filler is allocated at the interface of the two polymers.

Table 3.1 presents a summary of the melt-flow index (MFI), density and surface properties of PLA, EVA and SCB. The results obtained help to deduce in which polymer will have the closest contact with the filler. Polymers with low viscosities are said to have the ability to accommodate high filler contents [1] during melt mixing, and this should contribute to SCB diffusing into the PLA phase, because PLA has a higher MFI than EVA, which means that it has a lower viscosity. Mofokeng and Luyt [2] observed that the filler was dispersed in the polymer with the higher viscosity, which they explained in terms of the crystallinity of the polymer, where the filler will tend to locate itself on the polymer with lower crystallinity as the filler will locate itself in the amorphous phase of the polymer. As shown further on in this chapter, PLA (47% crystallinity) is more crystalline than EVA (10% crystallinity), and therefore the high crystallinity of PLA should discourage the location of SCB in EVA.

The surface energy values in Table 3.1 were used to calculate the interfacial tension values and wetting coefficient in Table 3.2 according to the geometric mean equation (Equation 3.1) [4-7].

$$\gamma_{12} = \gamma_1 + \gamma_2 - 2(\sqrt{\gamma_1^d \cdot \gamma_2^d} + \sqrt{\gamma_1^p \cdot \gamma_2^p}) \quad (3.1)$$

where γ_{12} = interfacial tension between components 1 and 2 in the blend, γ_1 and γ_2 are the total surface energies of components 1 and 2, γ_1^d and γ_2^d are the dispersive surface energies of components 1 and 2, and γ_1^p and γ_2^p are the polar surface energies of the components 1 and 2 in the composites. The calculated interfacial energy results indicate that the interfacial tension between EVA and SCB is higher than that between PLA and SCB. Although the interfacial tension is quite high in both cases (Table 3.2), it is lower for the PLA-SCB pair and therefore there is a slightly higher probability for SCB to have a greater affinity for PLA. The wetting coefficient ω_α was calculated from the Young's equation (Equation 3.2) [4-8].

$$\omega_\alpha = \frac{\gamma_{PLA/SCB} - \gamma_{EVA/SCB}}{\gamma_{PLA/EVA}} \quad (3.2)$$

where $\gamma_{PLA/SCB}$ is the interfacial tension between PLA and SCB, $\gamma_{EVA/SCB}$ is the interfacial tension between EVA and PLA, and $\gamma_{PLA/EVA}$ is the interfacial tension between PLA and EVA. If $\omega_\alpha < -1$, the particles are predicted to be located in polymer B, in this case EVA. If $\omega_\alpha > 1$, they are likely to be dispersed in polymer A, in this case PLA. If the value of ω_α is between -1 and 1, the particles are likely to disperse on the interface between the two polymers in the blend. In this case, $\omega_\alpha = 15.7$ which indicates that SCB will most likely be dispersed in the PLA phase.

Table 3.1 MFI, density and surface properties of PLA, EVA and SCB (values of SCB were obtained from literature [3])

Sample	Contact angle / deg		Surface energy / mN m ⁻¹			MFI / (g/10 min)	Density / g cm ⁻³
	H ₂ O	CH ₂ I ₂	γ	γ^d	γ^p		
PLA	63.1 ± 1.0	32.7 ± 0.4	52.8	43.1	9.7	8.3	1.25
EVA	69.7 ± 1.2	27.4 ± 0.4	51.3	45.3	6.1	1.2	0.94
SCB	38	39	51.9	17.8	34.2	-	-

γ = surface energy, γ^d = dispersive component of surface energy, γ^p = polar component of surface energy, MFI = melt flow index

Table 3.2 Interfacial tension and wetting coefficient of the investigated materials

Component couple	Interfacial tension / mN m^{-1} and wetting coefficient
PLA/EVA	0.3
PLA/SCB	12.9
EVA/SCB	17.6
ω_α	15.7

ω_α = wetting coefficient

To summarise, the lower viscosity of PLA, the lower interfacial tension between PLA and SCB, and the wetting coefficient of PLA/SCB being larger than 1, all suggest that SCB would preferably be in contact with PLA, despite PLA's relatively high crystallinity.

3.2 Morphology

3.2.1 Optical microscopy

Optical microscopy was used to examine both the morphologies as well as the dispersion of the fibres in the polymer matrices. Figure 3.1 shows the optical microscopy images of the PLA/EVA/SCB composites, Figure 3.2(a) shows that of the PLA/SCB composite, and Figure 3.2(b) that of the EVA/SCB composite. In general, the images in Figure 3.1 show a good dispersion of SCB fibres in the polymer blend matrices for all the composite samples. Even at high contents of SCB, good dispersion is observed with little agglomeration. The fibre lengths did not change during processing, indicating a low level of fibre damage during the composites preparation. A fairly good dispersion of SCB in the PLA matrix is observed in Figure 3.2(a), while Figure 3.2(b) shows that the fibre is strongly oriented and concentrated at the edge of the EVA sheet. Both these observations indicate that SCB has a stronger affinity for PLA.

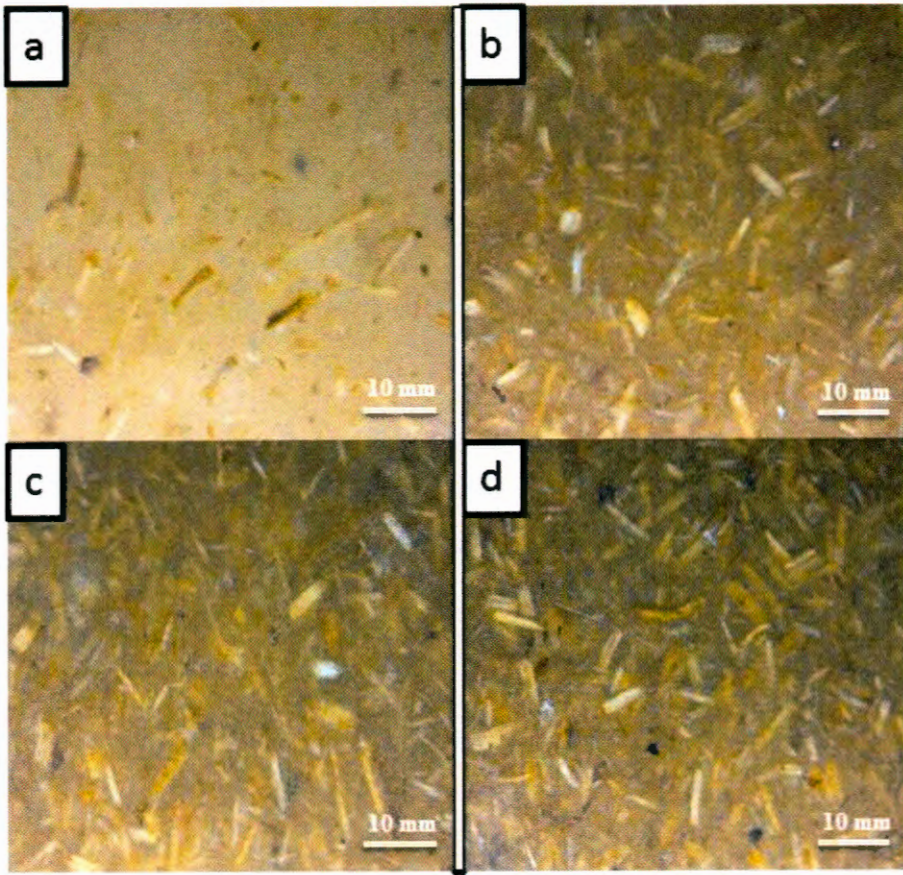


Figure 3.1 Optical microscopy pictures of (a) 66.5/28.5/5 w/w PLA/EVA/SCB, (b) 59.5/25.5/15 w/w PLA/EVA/SCB, (c) 56/24/20 w/w PLA/EVA/SCB and (d) 49/21/30 w/w PLA/EVA/SCB

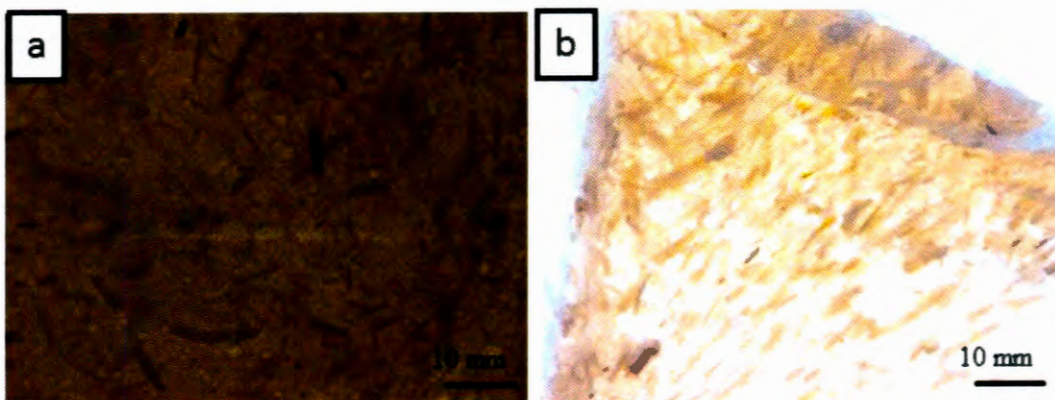


Figure 3.2 Optical microscopy images of (a) 80/20 w/w PLA/SCB, and (b) 80/20 w/w EVA/SCB

3.2.2 Scanning electron microscopy (SEM)

SEM was used to investigate the morphology and the possible interfacial adhesion between the polymers in the blends and the SCB fibre in the composites. The 50/50 w/w PLA/EVA blend in Figure 3.3(a) shows phase separation and a clear co-continuous morphology, though it is not possible to identify which phase is which directly from the SEM images. The image shows areas of brittle fracture (arrow A), that are probably PLA, and areas where plastic deformation is visible (arrow B), that are probably EVA. The samples were fractured under cryogenic conditions for 10 seconds. The time used was not long enough to bring the EVA sufficiently below its T_g to freeze all the molecular chain segments of the polymer, well PLA was already well below its T_g at room temperature. Under these conditions one could expect that EVA underwent ductile fracture, which showed up in the SEM images. The layer covering the fibre (arrow C in Figure 3.3(d)) is probably PLA because of the stronger affinity SCB has for PLA, as discussed in section 3.1. No fibre pull-outs were observed in the images, probably because of the good wetting of the fibre by PLA in the composites. However, some of the fibre ends were not covered by PLA (arrow D in Figures 3.3(c) and 3.3(h)) and therefore adsorption of the metal ions in contaminated water will probably take place at these fibre ends that are not smoothly covered by PLA. However, Figure 3.3(d) shows fibre ends covered by PLA, which may be detrimental for the effective removal of metal impurities from contaminated water. Large cavities are observed between the PLA and the EVA (Figures 3.3(a), 3.3(c) and 3.3(d)). These cavities are important for the contaminated water to diffuse through the composite and come into contact with the SCB fibre, where the metal impurities can be adsorbed.

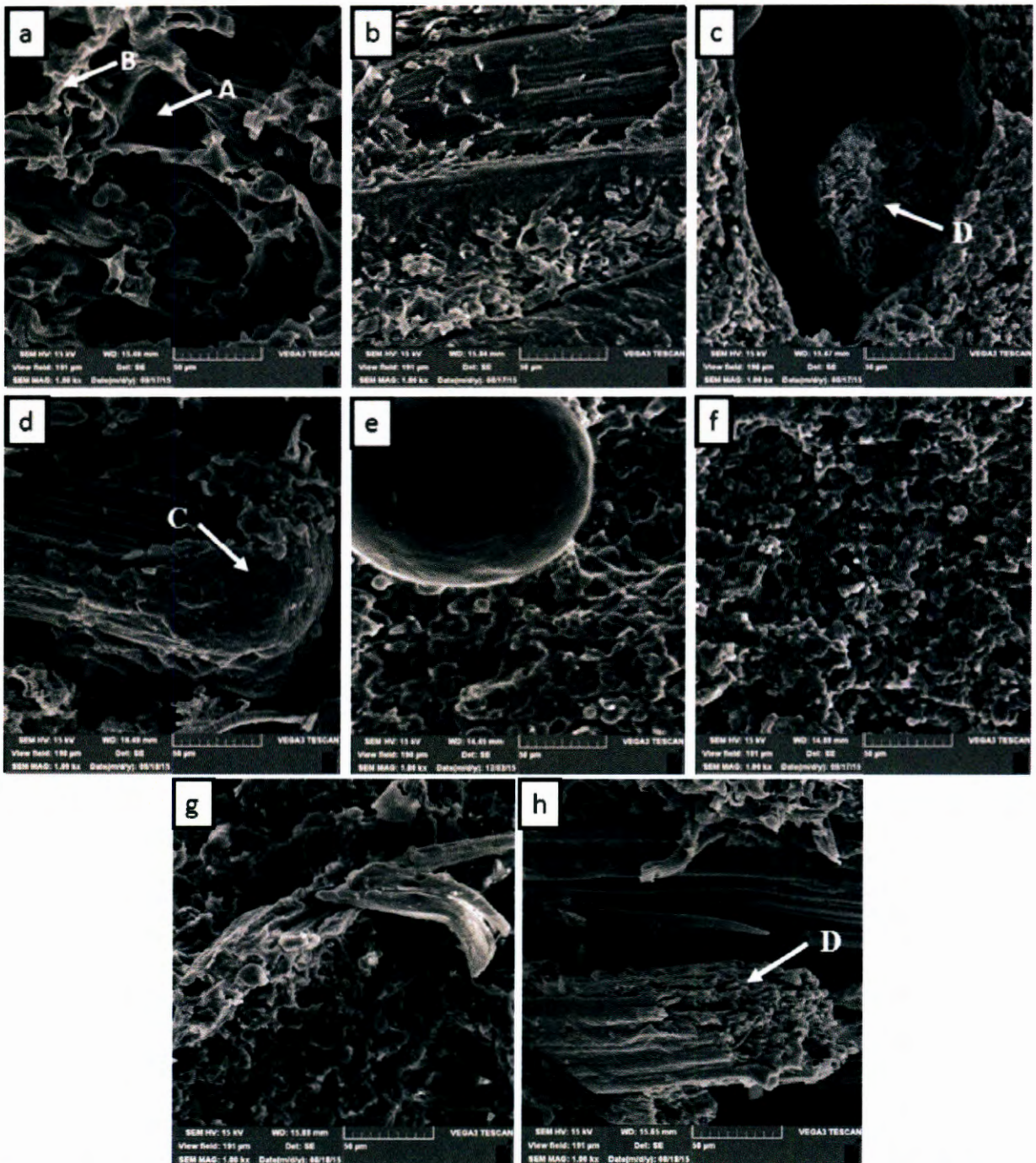


Figure 3.3 SEM images of the fractured surfaces of (a) 50/50 w/w PLA/EVA, (b) 47.5/47.5/5 w/w PLA/EVA/SCB, (c) 42.5/42.5/15 w/w PLA/EVA/SCB, (d) 35/35/30 w/w PLA/EVA/SCB,(e) 70/30 w/w PLA/EVA, (f) 66.5/28.5/5 w/w PLA/EVA/SCB, (g) 59.5/25.5/15 w/w PLA/EVA/SCB, and (h) 49/21/30 w/w PLA/EVA/SCB

3.2.3 Fourier-transform infrared (FTIR) spectroscopy

FTIR analyses were carried out to examine the possible interactions between the different components in the composites. Figure 3.4 represents the FTIR spectrum of the neat SCB, and this spectrum presents a typical cellulose spectrum [9-11]. The broad peak between 3412 and 3444 cm^{-1} is indicative of the existence of bound hydroxyl groups of macromolecular association (cellulose, pectin, and hemicellulose). The peaks observed at 2920 and 3930 cm^{-1} can be assigned to the C–H stretching for both cellulose and hemicellulose. The peaks around 1650 and 1750 cm^{-1} are indicative of the free and esterified carboxyl groups in hemicellulose. The peaks at 1457 cm^{-1} , 1370 cm^{-1} and 1030 cm^{-1} are for $-\text{CH}_3$ asymmetric, $-\text{CH}$ symmetric stretching, and $-\text{CH}$ aromatic stretching in lignin, respectively. The peak at 1315 cm^{-1} is for $-\text{CH}$ and C–O stretching of the acetyl group in hemicellulose. The peak at 896 cm^{-1} is for the glucosidic linkage [12-14].

The spectrum of pure EVA in Figure 3.5 shows absorption peaks around 2850 and 2920 cm^{-1} that correspond to the C–H asymmetric stretching vibrations in the polymer. The characteristic absorption peaks of the VA groups are as follows: 1736 cm^{-1} attributed to the stretching vibration of the $-\text{C}=\text{O}$ band; 1240 cm^{-1} attributed to the asymmetrical stretching vibration of the C–O band; 1030 cm^{-1} attributed to the symmetric stretching vibration of the COC band; 718 cm^{-1} attributed to the inner rocking vibration of methylene. The absorption peaks observed around 1439 cm^{-1} are largely attributed to the contributions from both VA and ethylene ($-\text{CH}_2$) units [15]. For neat PLA the absorption peaks at 2997 cm^{-1} and 2946 cm^{-1} are the $-\text{CH}_3$ asymmetric and symmetric stretching vibrations. The peak at 1749 cm^{-1} is for $-\text{C}=\text{O}$, those at 1452, 1382 and 1360 cm^{-1} the $-\text{CH}_3$ and $-\text{CH}$ bending vibrations, at 1266 cm^{-1} the stretching vibration of COC, those at 1181, 1127, and 1044 cm^{-1} the asymmetric and symmetric bending vibrations of COC as well as that of $-\text{CH}_3$ rocking, at 956 cm^{-1} the C–C stretching vibration, and at 867 cm^{-1} that of C–COO [16]. There does not seem to be any interaction between the functional groups of PLA and EVA, since there are no new peaks or significant peak shifts in the spectrum of the 50/50 w/w PLA/ EVA blend (Figure 3.5). This was to be expected since PLA and EVA have the same functional groups, except the ester group (C–COO) at 867 cm^{-1} that can only be seen for PLA. In the case of the PLA/SCB and EVA/SCB composites, if there was strong hydrogen bonding between PLA and SCB or EVA and SCB, confirmation of such hydrogen bonding may have been observed as a shift

in the carbonyl peak at 1750 cm^{-1} . However, no shift in this peak was observed, and therefore the FTIR analyses did not provide conclusive evidence of such hydrogen bonding between the -C=O group on PLA and EVA and the -OH group on SCB. Contrary to our own observations, Penjumras and co-workers [17] reported shifts of the C=O peak at 1753 cm^{-1} and the C-O peak at 1086 cm^{-1} for neat PLA to respectively 1770 cm^{-1} and 1090 cm^{-1} for PLA in biocomposites, which they attributed to the formation of hydrogen bonding between -OH in cellulose and C=O and C-O in PLA. Hydrogen bonding between the -C=O groups on PLA and EVA and the -OH group on SCB could also not be confirmed for 40/40/20 w/w PLA/EVA/SCB, since there was also no shift in the carbonyl peak at 1750 cm^{-1} for this composite.

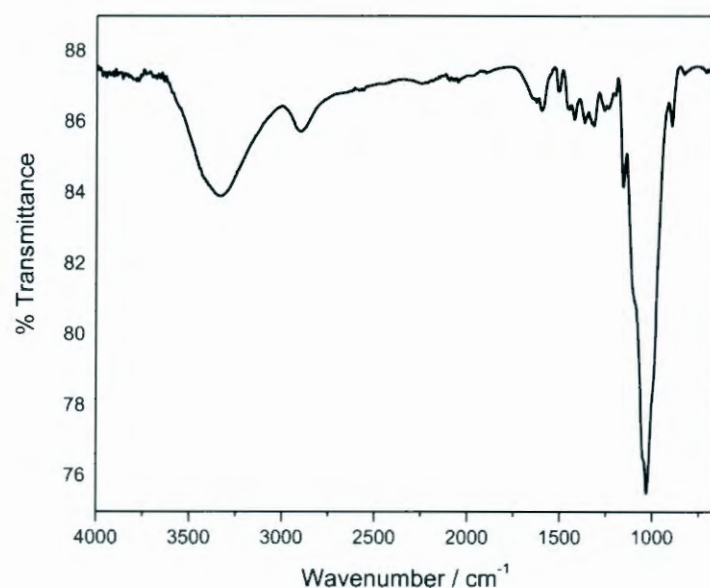


Figure 3.4 FTIR spectrum of SCB

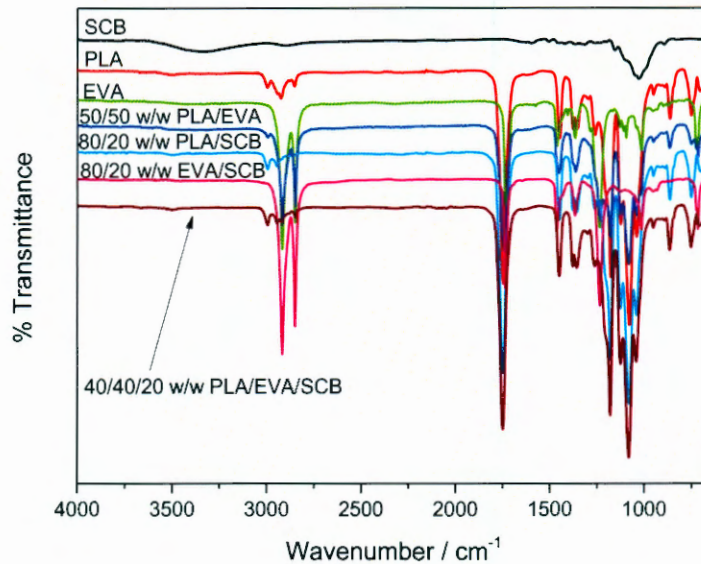


Figure 3.5 FTIR spectra of the PLA/EVA blend and the PLA/EVA/SCB bio-composites

3.3 Impact strength

Impact strength testing was used to analyse the mechanical properties of the PLA, EVA, PLA/EVA blends and the PLA/EVA/SCB composites. Figure 3.6 and Table 3.3 present the impact strength results of the investigated samples. The impact strength of EVA is larger than that of PLA. The reason is that EVA is a ductile polymer and PLA is a brittle polymer, and it is well known that brittle materials cannot impede crack propagation [18]. The 50/50 w/w PLA/EVA blend is expected to have good impact strength properties because it contains a high EVA content, but in this case the 70/30 w/w PLA/EVA blend has better impact strength properties. This is probably due to the fact that EVA formed small inclusions in the PLA matrix in the 70/30 w/w PLA/EVA blend, so that crazes initiated inside the polymer got terminated at the EVA inclusions, and cracks did not initially propagate through the polymer. The 50/50 w/w PLA/EVA had a co-continuous morphology with phase separation of the two polymers as seen in the previously discussed SEM images (section 3.2.2). The cracks between the two polymers will then develop and propagate along the interface between the two polymers.

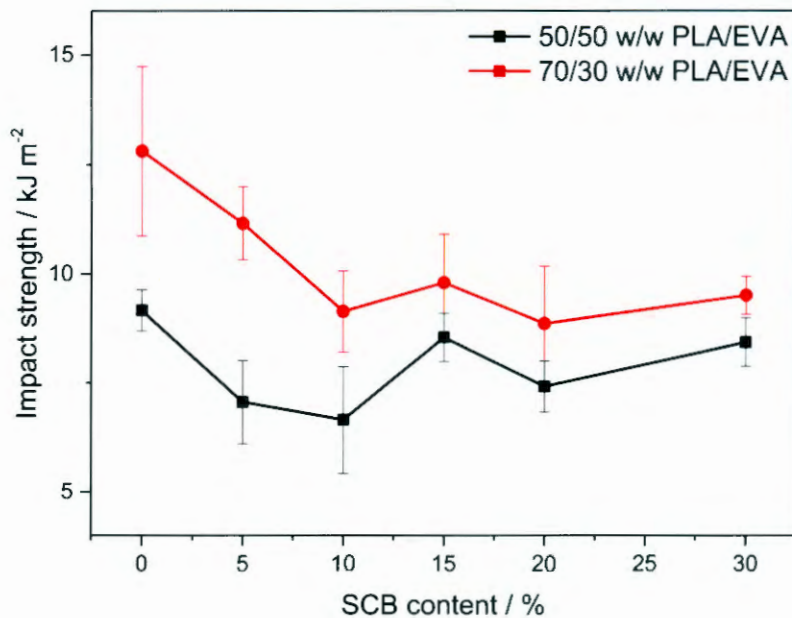


Figure 3.6 Impact strengths of the PLA/EVA blends and PLA/EVA/SCB composites at different SCB contents

The impact strength of the PLA/EVA/SCB composites decreased with an increase in SCB content for both blend compositions, which is not unexpected since the SCB particles probably acted as stress concentrators for the development of cracks. Different factors such as the fibre selection, matrix selection, interfacial strength, fibre dispersion, the interaction between the filler and the matrix, the fibre orientation, composite manufacturing, and porosity may contribute to the decrease in the mechanical properties of the composites [19,20]. In our case, the good interaction between the SCB and PLA in the blend matrix (section 3.1), combined with the weak interaction between PLA and EVA (section 3.2.2), probably played the biggest role in influencing the impact stress of the composites. As the SCB content increased, more interfacial voids/cavities were formed as a result of the separation between the PLA covered SCB and the EVA. Another reason might have been the fibre orientation within the matrix, since the best impact strength results are generally obtained for composites when the fibre is oriented perpendicular to the direction of impact [21]. In our case the fibres did not have a particular orientation (section 3.2.1), and therefore there was little resistance against crack propagation through the sample. Hatta and Akmar [22] also observed

a decrease in the impact strength of the composites and they concluded that their observations were the result of the fibre pull-out due to the low interfacial strength between the fibre and matrix.

Table 3.3 Impact properties of all the investigated samples

Sample	Impact strength / kJ m^{-2}
PLA	7.0 ± 1.0
EVA	*
50/50 w/w PLA/EVA	9.2 ± 0.5
47.5/47.5/5 w/w PLA/EVA/SCB	7.1 ± 1.0
45/45/10 w/w PLA/EVA/SCB	6.7 ± 1.2
42.5/42.5/15 w/w PLA/EVA/SCB	8.5 ± 0.6
40/40/20 w/w PLA/EVA/SCB	7.4 ± 0.6
35/35/30 w/w PLA/EVA/SCB	8.4 ± 0.7
70/30 w/w PLA/EVA	12.8 ± 1.9
66.5/28.5/5 w/w PLA/EVA/SCB	11.2 ± 0.8
63/27/10 w/w PLA/EVA/SCB	9.1 ± 0.9
59.5/25.5/15 w/w PLA/EVA/SCB	9.8 ± 1.1
56/24/20 w/w PLA/EVA/SCB	8.9 ± 1.3
49/21/30 w/w PLA/EVA/SCB	9.5 ± 0.4

* Under the analysis conditions, EVA did not break

3.4 Thermal analysis

3.4.1 Thermogravimetric analysis (TGA)

The TGA was used to determine the thermal stability of all the investigated samples. In the case of the PLA, the TGA curve shows one degradation step at 351 °C that is the main chain decomposition (Figure 3.7). EVA shows two degradation steps at 356 and 460 °C related to the removal of acetyl groups and the main chain decomposition, respectively [23,24]. The SCB fibre shows three degradation steps. The first step below 100 °C corresponds to the evaporation of moisture from the sample, while the step around 337 °C corresponds to the thermal decomposition of hemicellulose and the glycosidic links of cellulose. The step around 455 °C is the result of the thermal decomposition of non-cellulosic substances such as lignin [25-27]. SCB normally forms a char that is the result of the exothermic reaction between the glycolaldehyde and levoglucosan formed by the decomposition of cellulose [28]. In our case, however, there was no thermally stable residue up to the maximum temperature of the analysis.

The PLA/EVA blends and PLA/EVA/SCB composites show two decomposition steps (Figure 3.8). The first step is a combination of PLA degradation, EVA deacetylation, and the first main step of the SCB degradation. The second step is a combination of the degradation of the EVA backbone and the lignin from the SCB. The presence of SCB generally decreases the thermal stability of the composite samples (Table 3.4) because of the lower thermal stability of the fibre. However, the thermal stability of the composites is higher than that of the SCB, because the higher thermal stability polymer matrix protects the SCB from decomposing at its usual decomposition temperature.

It is known that after the deacetylation of EVA, polyene is formed, the degradation of which gives rise to the formation of aromatic and aliphatic volatiles, CO₂ and H₂O. The aromatic volatiles originate from the deacetylated VAc entities, while the aliphatic volatiles are formed by the chain scission reactions in polyene [29]. The SCB char probably delays the degradation of polyene in the composites, or the diffusion of the volatile (aromatic and aliphatic) degradation products out of the degrading sample, which is seen as an increase in the temperature of the mass loss step between 400 and 500 °C with an increase in SCB content.

Table 3.4 TGA results for investigated samples

Sample	T ₁ / °C	T ₂ / °C
PLA	350.7	
EVA	355.7	460.2
SCB	336.9	455.0
50/50 w/w PLA/EVA	366.3	472.2
47.5/47.5/5w/w PLA/EVA/SCB	350.6	467.8
45/45/10w/w PLA/EVA/SCB	352.1	466.2
42.5/42.5/15w/w PLA/EVA/SCB	345.5	476.7
40/40/20w/w PLA/EVA/SCB	335.0	480.34
35/35/30w/w PLA/EVA/SCB	326.1	482.6
70/30 w/w PLA/EVA	362.6	475.9
66.5/28.5/5w/w PLA/EVA/SCB	349.9	474.4
63/27/10w/w PLA/EVA/SCB	347.7	480.3
59.5/25.5/15w/w PLA/EVA/SCB	335.0	481.1
56/24/20w/w PLA/EVA/SCB	332.0	479.6
49/21/30w/w PLA/EVA/SCB	320.0	475.2

T₁ and T₂ are the temperatures of the peak maxima of the first and second peak in the derivative TGA curves

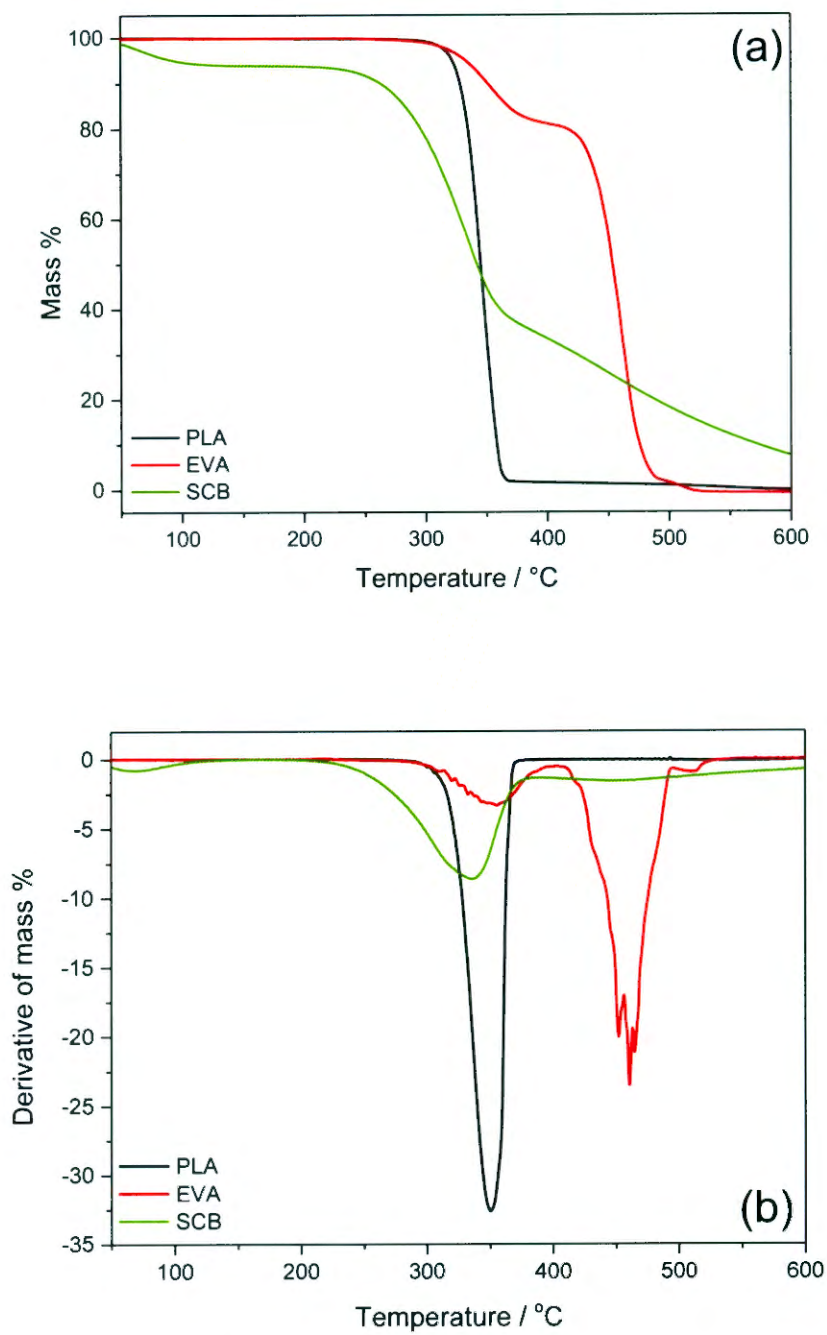


Figure 3.7 (a) TGA and (b) derivative TGA curves of PLA, EVA and SCB

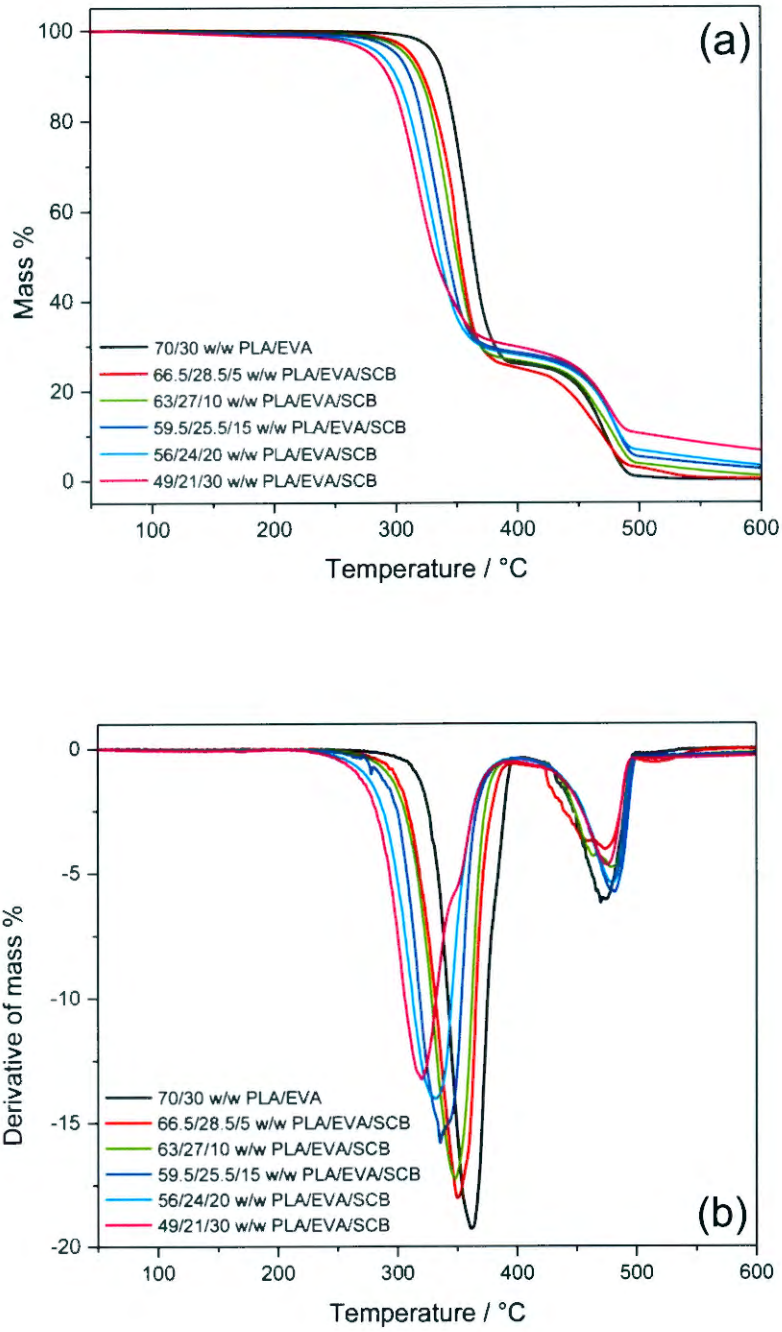


Figure 3.8 (a) TGA and (b) derivative TGA curves of 70/30 w/w PLA/EVA and its bio-composites

3.4.2 Differential scanning calorimetry

DSC analysis was performed to characterize the thermal behaviour of the samples used in this investigation. All the reported DSC heating results were obtained from the second scan to eliminate the effect of thermal history. The normalised melting and crystallization enthalpy values shown in Tables 3.5 and 3.6 were determined according to Equations 3.3 and 3.4.

$$\Delta H_m^n = \Delta H_m/w \quad (3.3)$$

$$\Delta H_c^n = \Delta H_c/w \quad (3.4)$$

where ΔH_m^n and ΔH_c^n are the melting and crystallization enthalpies normalised with respect to the amount of the respective polymer in the sample, ΔH_m and ΔH_c are the melting and crystallization enthalpies of the respective polymers, and w is the mass fraction of that polymer in the blend or composite.

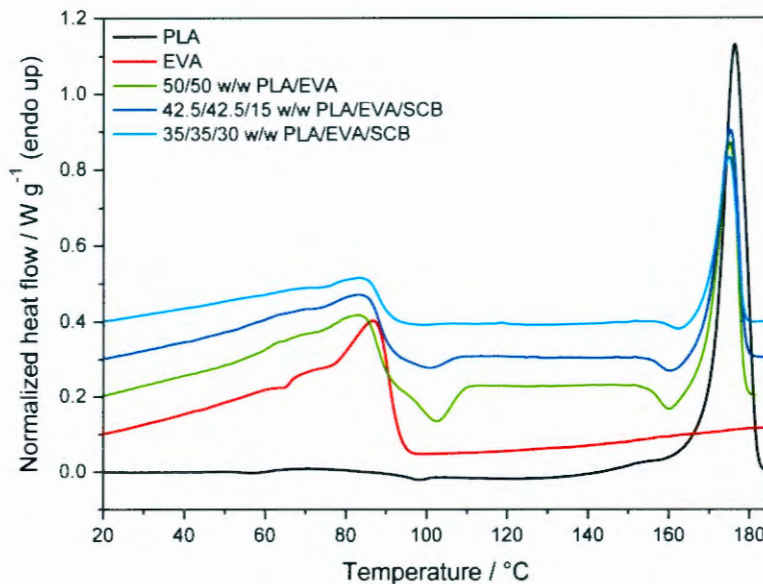


Figure 3.9 DSC second heating curves of the neat PLA, neat EVA, the 50/50 PLA/EVA blend and composites based on this blend

The PLA shows a melting temperature of 176 °C and a crystallization temperature of 131 °C, and it does not show any cold crystallization exotherms (Figure 3.9). There is also a good correlation between its crystallization and melting enthalpies (Table 3.6), which indicates that the polymer crystallized completely on cooling. The same is true for EVA that melts around 87 °C and crystallizes around 70 °C (Table 3.5). The PLA/EVA blends show two melting peaks at approximately the same temperatures as those of the neat polymers, which confirms the complete immiscibility of PLA and EVA at all the investigated compositions.

In the 50/50 w/w PLA/EVA blend (figure 3.9) the heating curve shows two crystallization exotherms, one just after the melting of EVA and the other one just before the melting of PLA. These may be related to the re-crystallization of a fraction of the molten EVA, cold crystallization of the PLA amorphous fractions because of more free volume created by the molten EVA, or co-crystallization of certain EVA and PLA fractions. Inspection of the different melting and crystallization enthalpies shows that there are significant differences between the melting and crystallization enthalpies of EVA in the blend. The sum of the cold crystallization enthalpies and the PLA crystallization enthalpy is also not equal to the melting enthalpy of PLA in the blend. These discrepancies indicate that the crystallization and melting of respectively EVA and PLA in the 50/50 w/w PLA/EVA blend are influenced in a complex way by the presence of the other polymer.

In the case of the 70/30 w/w PLA/EVA blend (Figure 3.10) the first cold crystallization exotherm is absent. This is probably related to the morphology of this blend compared to that of the 50/50 w/w PLA/EVA blend. The 50/50 w/w PLA/EVA blend has a co-continuous morphology, while in the 70/30 w/w PLA/EVA blend the EVA is dispersed as spheres in the PLA continuous phase as observed in the SEM photos (section 3.2.2).

The presence of the fibre in the composites also has an influence on the appearance of the cold crystallization peaks, although this influence cannot be directly related to the polymer ratio or the amount of fibre in the respective composites. Since PLA is expected to be more attracted to the fibres, the crystallization of the PLA on the fibre surfaces, and changes in the morphology as a result of this, may influence the crystallization during heating in a complex way.

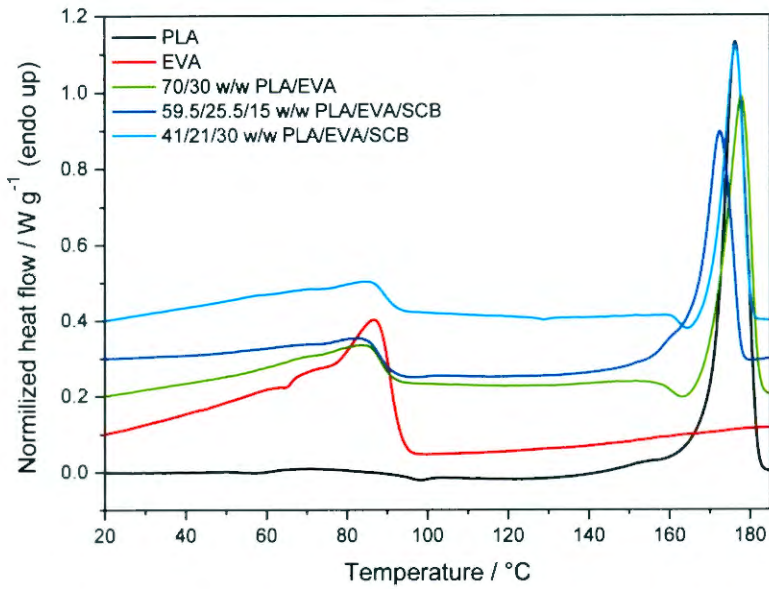


Figure 3.10 DSC second heating curves of the neat PLA, neat EVA, the 70/30 PLA/EVA blend and composites based on this blend

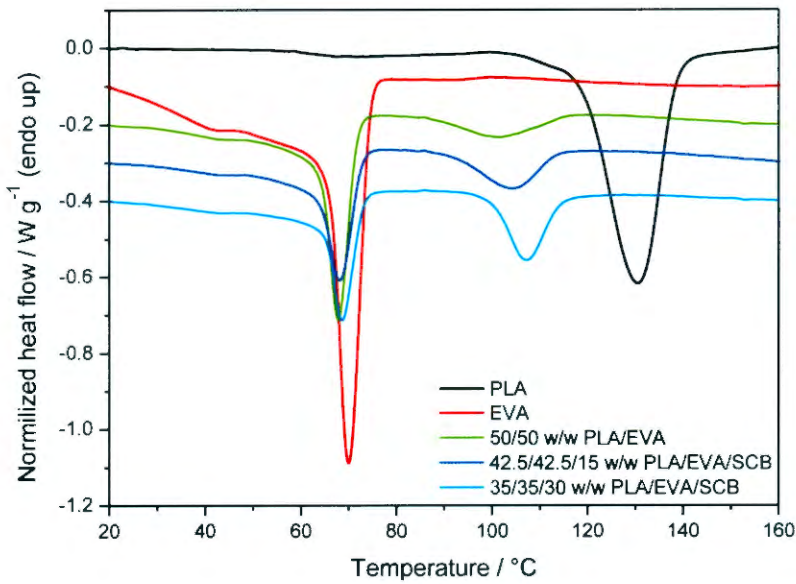


Figure 3.11 DSC cooling curves of the neat PLA, neat EVA, the 50/50 PLA/EVA blend and composites based on this blend

In comparing the normalised melting enthalpies of PLA in the different samples, there are differences but no trend, and one can therefore conclude that neither blending, nor the ratio of the polymers in the blends, nor the presence and amount of fibre in the composites, had a significant influence on the crystallinity of PLA. The same can be said for the EVA crystallinity.

The crystallization temperature of PLA is around 131 °C and that of EVA around 70 °C (Tables 3.5 and 3.6). The PLA/EVA blend shows two crystallization peaks, which confirms the immiscibility of the two polymers. Inspection of the cooling curves shows little change in the crystallization temperatures of EVA (Figures 3.11 and 3.12), which means that neither the presence of crystallized PLA nor the presence of fibre had an influence on the crystallization behaviour of EVA. PLA, on the other hand, crystallized at significantly lower temperatures, probably because the molten EVA acts like a plasticizer and creates more free volume for the movement of the PLA chains.

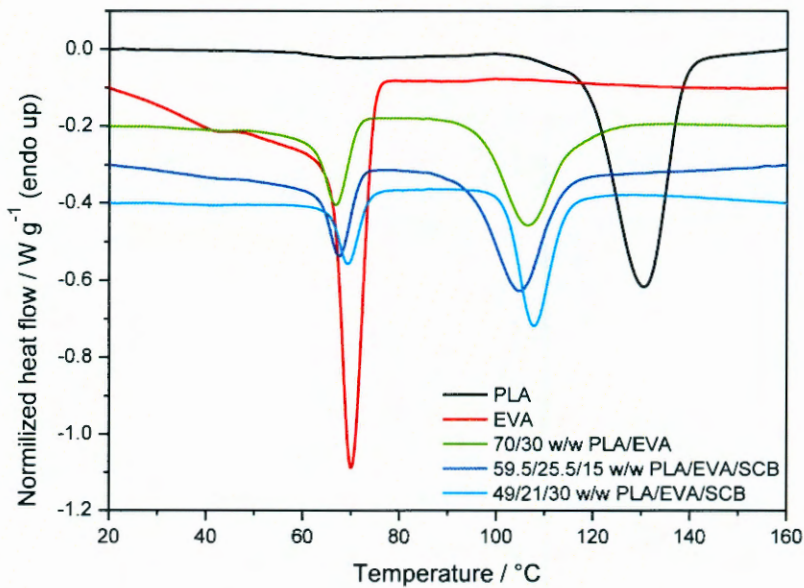


Figure 3.12 DSC cooling curves of the neat PLA, neat EVA, the 70/30 PLA/EVA blend and composites based on this blend

Table 3.5 Melting and crystallization temperatures and enthalpies of EVA in the blends and composites

Sample	$T_c / ^\circ\text{C}$	$\Delta H_c / \text{J g}^{-1}$	$\Delta H_c^n / \text{J g}^{-1}$	$T_m / ^\circ\text{C}$	$\Delta H_m / \text{J g}^{-1}$	$\Delta H_m^n / \text{J g}^{-1}$
EVA	70.2 ± 0.1	28.2 ± 0.4	28.2	87.4 ± 0.3	27.2 ± 1.3	27.2
50/50 w/w PLA/EVA	67.7 ± 0.2	18.6 ± 2.8	37.2	84.7 ± 0.7	12.6 ± 1.4	25.2
42.5/42.5/15 w/w PLA/EVA/SCB	68.4 ± 0.2	13.3 ± 0.7	31.3	85.5 ± 0.0	10.9 ± 1.2	25.6
35/35/30 w/w PLA/EVA/SCB	68.3 ± 0.4	10.4 ± 0.8	29.7	85.5 ± 0.0	10.1 ± 0.6	28.9
70/30 w/w PLA/EVA	66.9 ± 0.2	8.6 ± 0.4	28.7	85.4 ± 0.4	7.8 ± 0.2	26.0
59.5/25.5/15 w/w PLA/EVA/SCB	67.7 ± 0.3	7.5 ± 0.1	29.4	84.7 ± 0.9	8.5 ± 0.5	33.3
49/21/30 w/w PLA/EVA/SCB	69.3 ± 0.1	6.0 ± 0.3	28.6	86.5 ± 0.9	5.6 ± 1.2	26.7

T_m - melting peak temperature; ΔH_m – melting enthalpy; ΔH_m^n – melting enthalpy normalised with respect to amount of EVA; T_c – crystallization peak temperature, ΔH_c – crystallization enthalpy, ΔH_c^n –crystallization enthalpy normalised with respect to amount of EVA

Table 3.6 Melting and crystallization temperatures and enthalpies of PLA in the blends and composites

Sample	$T_c/^\circ\text{C}$	$\Delta H_c/\text{J g}^{-1}$	$\Delta H_c^n/\text{J g}^{-1}$	$T_{cc1\text{PLA}}/^\circ\text{C}$	$\Delta H_{cc1}/\text{J g}^{-1}$	$\Delta H_{cc1}^n/\text{J g}^{-1}$	$T_{cc2}/^\circ\text{C}$	$\Delta H_{cc2}/\text{J g}^{-1}$	$\Delta H_{cc2}^n/\text{J g}^{-1}$	$T_m/^\circ\text{C}$	$\Delta H_m/\text{J g}^{-1}$	$\Delta H_m^n/\text{J g}^{-1}$
PLA	131.1 ± 0.7	43.6 ± 3.6	43.6	-	-	-	-	-	-	176.4 ± 0.1	46.9 ± 0.2	46.9
50/50 w/w PLA/EVA	102.7 ± 1.1	6.7 ± 0.3	13.4	102.4 ± 0.3	5.2 ± 1.4	10.4	159.6 ± 0.2	2.1 ± 0.6	4.2	174.8 ± 0.4	24.5 ± 0.6	49.0
42.5/42.5/15 w/w PLA/EVA/SCB	104.8 ± 0.4	8.6 ± 0.7	20.2	101.1 ± 0.8	1.7 ± 0.3	4.0	160.9 ± 0.4	1.6 ± 0.3	3.8	175.7 ± 0.4	21.3 ± 1.1	50.1
35/35/30 w/w PLA/EVA/SCB	107.0 ± 0.2	10.3 ± 0.5	29.4	-	-	-	162.5 ± 0.1	0.7 ± 0.1	2.0	174.9 ± 0.2	16.0 ± 0.6	45.7
70/30 w/w PLA/EVA	106.6 ± 0.3	24.4 ± 1.2	34.9	-	-	-	163.3 ± 0.8	2.3 ± 0.4	3.3	177.7 ± 0.8	32.1 ± 0.7	45.9
59.5/25.5/15 w/w PLA/EVA/SCB	105.7 ± 1.0	21.9 ± 0.9	36.8	-	-	-	-	-	-	172.6 ± 0.2	33.9 ± 0.6	57.0
49/21/30 w/w PLA/EVA/SCB	107.6 ± 0.1	18.3 ± 0.7	37.3	-	-	-	165.0 ± 0.5	0.9 ± 0.3	1.8	176.8 ± 0.4	24.6 ± 0.8	50.2

T_m – melting peak temperature; T_{cc} – cold crystallization temperature; ΔH_m – melting enthalpy; ΔH_{cc} – cold crystallization enthalpy; ΔH_m^n – melting enthalpy normalised with respect to amount of PLA; ΔH_{cc}^n –cold crystallization enthalpy normalised with respect to amount of PLA; T_c – crystallization peak temperature; ΔH_c – crystallization enthalpy; ΔH_c^n –crystallization enthalpy normalised with respect to PLA; 1 and 2 after cc indicate first and second cold crystallization peak

3.5 Water absorption

Water absorption analysis was used to assess the absorption efficiency of the PLA/EVA/SCB composites. The amount of water absorbed in the composites was calculated from the weight difference between the samples exposed to water and the initially weighed samples (Equation 3.5) [30-33].

$$\%W = \frac{W_t - W_i}{W_i} \times 100 \quad (3.5)$$

where %*W* is the percentage water absorbed, *W_t* is the final weight of the sample after a certain time *t* of water immersion, and *W_i* is the initial sample mass. It was found by other researchers [30-34] that there are three ways in which water molecules can enter polymer composites, i.e. diffusion, capillary transport and transport due to micro-cracks/micro-voids. In our case, micro-cracks/micro-voids was the most probable mode of water absorption by the composites, because of the obvious voids observed in the SEM photos of the investigated samples (section 3.2.2).

Both graphs in Figure 3.13 depict an increase in water absorption with an increase in SCB loading. This is due to more hydrophilic fibre introduced in the composites, since the absorbed water will be retained in the inter-fibrillar space of the cellulosic structure of the filler, as well as in the interface and micro-voids present in the composites. Another observation is that the composites prepared from the 50/50 w/w PLA/EVA blend absorbed more water than those prepared from the 70/30 w/w PLA/EVA blend. This is due to the weak interaction between the two polymers (section 3.2.2) resulting in more voids/cavities in the 50/50 w/w PLA/EVA blend that will more easily transport the water to the fibres, and in which more water will be trapped.

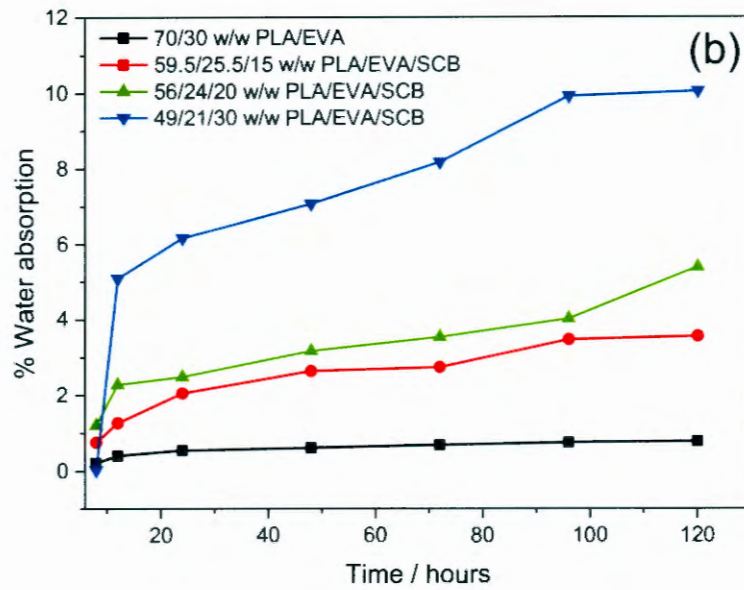
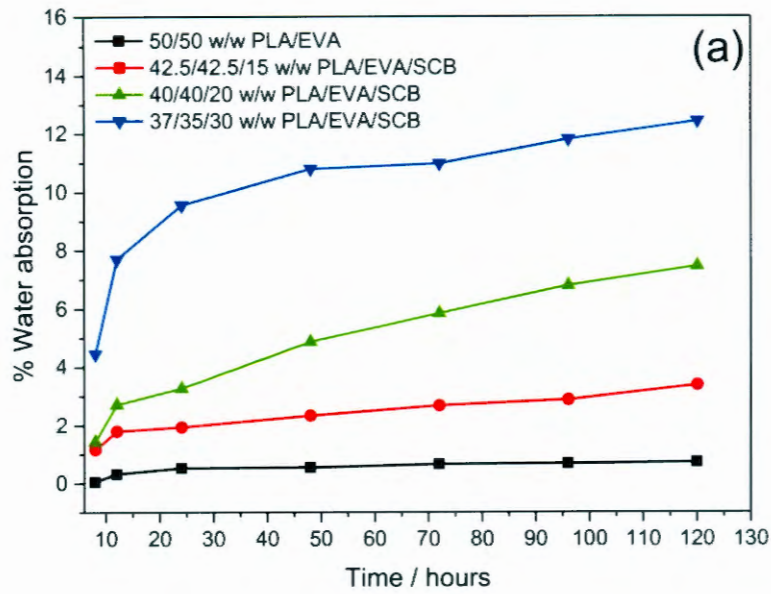


Figure 3.13 Water absorption curves of the blends and composites based on (a) 50/50 and (b) 70/30 w/w PLA/EVA

3.6 Atomic absorption spectroscopy (AAS)

AAS analysis was used to determine the adsorption capacity of SCB fibre and the PLA/EVA/SCB composites on aqueous media. Natural fibres were used for metal adsorption because of their functional groups seen in FTIR (section 3.2.3) that have an affinity for metal complexation. In our case, metal complexation and micro cracks in the composites (observed in the SEM photos (section 3.2.2)) will both contribute to the effective removal of lead from water. Different parameters have been evaluated in the adsorption capacity of SCB and the PLA/EVA/SCB composites i.e. initial concentration, pH level and the contact time. The normalised adsorption values shown in Tables 3.7 to 3.9 were determined according to Equation 3.6.

$$C_a^n = C_a / (w_f w_s) \quad (3.6)$$

where C_a^n is the concentration adsorbed normalised to the amount of the pure SCB in the sample, and to the mass of sample used in the test, C_a is the concentration adsorbed, w_f is the mass fraction of SCB in the composite, and w_s is the sample mass used in the test.

Normally one would not expect the PLA/EVA/SCB composites to adsorb more lead than the pure SCB fibre, because the fibre in the composites is covered by polymer, and the only access to the fibre is through the micro cracks in the composites. However, inspection of the values in Tables 3.7 to 3.9 shows that in some cases more metal was removed by the composites than by the neat fibre. Possible reasons for this observation are that (i) it was difficult to completely immerse the fibre, which formed the control samples, in the metal ion solution and they could therefore not optimally adsorb the metal ions from the solution, and (ii) metal ions could have been adsorbed onto the polymer surfaces through their interaction with the functional groups on the polymer chains. The 50/50 w/w PLA/EVA samples have a more co-continuous morphology than the 70/30 w/w PLA/EVA samples. They should therefore have more continuous pathways between the two incompatible polymers that should allow more effective penetration of the solution to reach the fibres in the composite. However, inspection of the values in Table 3.7 shows that this is not necessarily true, and there is no direct correlation between the amounts of metal removed from the solutions and the respective composite morphologies.

The concentration adsorbed by neat SCB increased with an increase in initial metal concentration in the solution, but approaches saturation at the higher initial concentrations (Table 3.7). This may be due to a limited number of adsorption sites on the fibre that are saturated at a certain metal ion concentration. Above this concentration the fibre does not adsorb more metal ions if mono-layer adsorption takes place. Based on the results for neat SCB, one would expect an increase in the adsorption of the metal impurities with an increase in the initial concentration in the composites as well. However, this was not generally observed (see values marked with an asterisk in Table 3.7), and it was not possible to repeat the analyses. However, a higher adsorption values was observe for the 400 ppm solution, which was expected due to the larger amount of metal impurities available for adsorption. In the case of the composites the efficiency of water diffusion through the sample (which is determined by the sample morphology and presence of micro-cracks), and the extent to which the SCB is exposed to these micro-cracks, play a much more dominant role.

Table 3.7 AAS results of all investigated samples at different initial concentrations

Samples (w/w PLA/EVA/SCB)	Initial Pb concentration / ppm	Adsorbent sample mass (w) / g	Concentration Pb adsorbed (C_a) / ppm	Concentration Pb adsorbed, normalised to amount of fibre in sample and amount of sample used in test (C_a^n) / ppm g ⁻¹
0/0/100	100	0.5	80.4	160.8
0/0/100	200	0.5	177.5	355.0
0/0/100	300	0.5	233.2	466.4
0/0/100	400	0.5	242.0	484.0
42.5/42.5/15	100	2.0115	52.8	175.0
42.5/42.5/15	200	2.0625	49.9*	161.3*
42.5/42.5/15	300	2.0195	52.0*	171.7*
42.5/42.5/15	400	2.0890	215.3	712.6
35/35/30	100	2.0040	80.9	134.6
35/35/30	200	2.0729	52.8*	84.9*
35/35/30	300	2.0642	63.9*	103.2*
35/35/30	400	2.0494	212.9	340.4
59.5/25.5/15	100	2.0452	82.8	269.9
59.5/25.5/15	200	2.0806	77.5*	248.3*
59.5/25.5/15	300	2.0676	75.2*	242.5*
59.5/25.5/15	400	2.0188	272.5	899.9
49/21/30	100	2.0607	90.5	146.4
49/21/30	200	2.0958	75.9*	120.7*
49/21/30	300	2.0545	47.1*	76.4*
49/21/30	400	2.0665	288.7	475.3

At different initial concentrations, pH 5 and 5 hour of contact time were used.

It is observed (Table 3.8) that the C_a^n values are of the same order of magnitude for the same sample composition, with no trend in the extent of adsorption. At least one value (marked with an asterisk) was too high to make sense in this system. With this system as well, the efficiency of water diffusion through the sample (which is determined by the sample morphology and the presence of micro-cracks), the extent to which the SCB is exposed to these micro-cracks, and possible adsorption on the surfaces of the matrix polymers, probably played a much more dominant role, although the hydronium ions (H_3O^+) in the lower pH solutions may have influenced the adsorption efficiency. The metal ions will have to compete with these hydronium ions for the adsorbent sites, or the functional groups in SCB may be protonated at these pH levels, and hence rendered unavailable for ion exchange and complexation with the metal ions. At the higher pH levels the metal ions may start to precipitate, which will reduce the efficiency of using SCB as an adsorbent.

Table 3.8 AAS results of all investigated samples at different pH level

Samples (w/w PLA/EVA/SCB)	pH	Adsorbent sample mass (w) / g	Concentration Pb adsorbed (C_a) / ppm	Concentration Pb adsorbed, normalised to amount of fibre in sample and amount of sample used in test (C_a^n) / ppm g ⁻¹
0/0/100	3	0.5	232.8	465.6
0/0/100	5	0.5	242.0	484.0
0/0/100	7	0.5	211.5	423.0
0/0/100	9	0.5	195.2	390.4
42.5/42.5/15	3	2.0792	200.0	641.3
42.5/42.5/15	5	2.0142	215.3	712.6
42.5/42.5/15	7	2.0966	189.4	602.2
42.5/42.5/15	9	2.0535	173.7	563.9
35/35/30	3	2.0018	174.8	291.1
35/35/30	5	2.0872	212.9	340.0
35/35/30	7	2.0428	174.8	285.2
35/35/30	9	2.0614	160.5	259.5
59.5/25.5/15	3	2.1018	111.6	354.0
59.5/25.5/15	5	2.0188	272.5	899.9*
59.5/25.5/15	7	2.0451	66.9	218.1
59.5/25.5/15	9	2.0188	53.9	171.4
49/21/30	3	2.0473	97.9	159.4
49/21/30	5	2.0665	288.7	475.3
49/21/30	7	2.0837	67.8	108.5
49/21/30	9	2.0335	39.1	64.1

At different pH levels, 400 ppm initial concentration was used and 5 hours contact time.

An increase in the contact time generally resulted in an increase in the concentration per gram adsorbed (Table 3.9) for the composites, although the increase is fairly slow between 60 and 300 minutes. The diffusion of water is obviously relatively slow through the micro-cracks in the blend composite samples, with the optimum adsorption being reached at times longer than

60 minutes of insertion in the metal ion solution. Contact time had little influence on the adsorption efficiency of the neat fibre, although a slight increase was observed. This is probably due to some penetration of the water in between the fibre fibrils that allowed access to some hidden adsorption sites.

Table3.9 AAS results of all investigated samples at different contact time

Samples (w/w PLA/EVA/SCB)	Contact time (min)	Adsorbent sample mass (w) / g	Concentration Pb adsorbed (C_a) / ppm	Concentration Pb adsorbed, normalised to amount of fibre in sample and amount of sample used in test (C_a'') / ppm g ⁻¹
0/0/100	30	0.5	206.5	413.0
0/0/100	60	0.5	211.4	422.8
0/0/100	180	0.5	217.3	434.6
0/0/100	300	0.5	242.0	484.0
42.5/42.5/15	30	2.0258	40.4	133.0
42.5/42.5/15	60	2.0427	183.3	598.2
42.5/42.5/15	180	2.0541	207.2	672.5
42.5/42.5/15	300	2.0334	215.3	712.6
35/35/30	30	2.08	58.5	93.8
35/35/30	60	2.0228	189.8	312.8
35/35/30	180	2.0532	195.2	316.9
35/35/30	300	2.0523	212.9	340.0
59.5/25.5/15	30	2.1144	30.6	96.5
59.5/25.5/15	60	2.1096	163.3	516.1
59.5/25.5/15	180	2.006	191.9	637.8
59.5/25.5/15	300	2.0188	272.5	899.9*
49/21/30	30	2.0314	151.2	248.1
49/21/30	60	2.0372	256.6	419.9
49/21/30	180	2.0456	274.1	446.6
49/21/30	300	2.0665	288.7	475.3

At different contact times, initial concentration used was 400 ppm and 5 pH level

It is observed from the results above that not only the SCB within the composites is responsible for the adsorption of the metal impurities, since the results on the composites show values comparable to or even higher than that of pure SCB. Some of the metal impurities probably remain trapped inside the cavities/voids and one or both of the polymers could have played a role in the metal complexation process, since both polymers do have functional groups that could interact with and adsorb the metal impurities.

Adsorption isotherms

An adsorption isotherm equation is an expression of the relation between the amount of solute adsorbed and the concentration of the solute in the fluid phase, and it is important in describing how adsorbates will interact with adsorbents, and so is critical for design purposes. Two

isotherm equations were adopted in this study, the Freundlich and Langmuir isotherms. The equilibrium adsorption capacity q_e (mg g^{-1}) was calculated according to Equation 3.8 [35-42]:

$$q_e = \frac{(C_o - C_e)}{w_a} \times V \quad (3.8)$$

where C_o and C_e (ppm or mg L^{-1}) were the initial and final concentrations of lead, respectively. V (L) is the volume of the solution, and w_a (g) is the actual mass of SCB used.

Freundlich

The Freundlich sorption isotherm, one of the most widely used mathematical descriptions, gives an expression encompassing the surface heterogeneity and the exponential distribution of active sites and their energies.

The Freundlich isotherm is defined as [35-42]:

$$q_e = K_F C_e^{\frac{1}{n}} \quad (3.9)$$

and the linearized form is:

$$\log q_e = \log K_F + \left(\frac{1}{n}\right) \log C_e \quad (3.10)$$

where C_e is the equilibrium concentration in mg L^{-1} (AAS reading after removing immersed sample), q_e is the amount of adsorbate adsorbed per unit weight of adsorbent mg g^{-1} , K_F is a parameter related to the temperature, and n is a characteristic constant for the adsorption system studied. The value of n indicates a favourable adsorption when $1 < n < 10$, and it is more favourable if $1/n < 1$. The plots of $\log Q_e$ against $\log C_e$ are shown in Figure 3.14. The Freundlich isotherm constants and their correlation coefficients R^2 are listed in Table 3.10. It is not possible to put a straight line through the values of pure SCB in the graph, so the Freundlich isotherm cannot describe these points, probably because adsorption did not take place heterogeneously on the fibre surface. This was confirmed when applying the Langmuir isotherm, which assumes monolayer adsorption and which fitted the data much better.

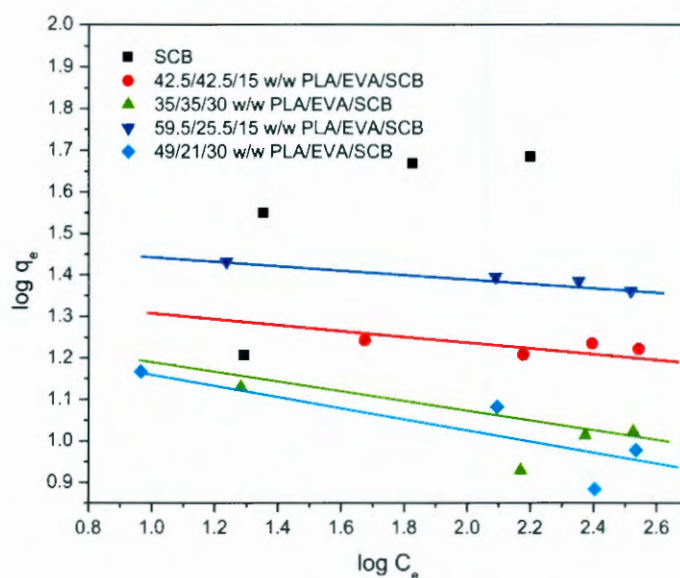


Figure 3.14 Freundlich plots from which the data in Table 3.7 were obtained

Table 3.10 Freundlich isotherm constants for the sorption of lead Pb(II) ions by the different composite samples

Samples (w/w PLA/EVA/SCB)	Freundlich constants		
	K_F	n	R^2
0/0/100	-	-	-
42.5/42.5/15	18.6209	-50.5051	0.2310
35/35/30	17.3301	-9.9899	0.4906
59.5/25.5/15	31.2536	-20.0803	0.9442
49/21/30	20.8593	-6.8446	0.7173

Langmuir

The Langmuir equation is based on the assumptions that maximum adsorption corresponds to a saturated mono-layer of adsorbate molecules on the adsorbent surface, that the energy of adsorption is constant, and that there is no transmigration of adsorbate in the plane of the surface.

The Langmuir isotherm is defined as [35-42]:

$$q_e = \frac{(b q_m C_e)}{(1 + b C_e)} \quad (3.11)$$

and the linearized form is:

$$\frac{C_e}{q_e} = \left(\frac{C_e}{q_m}\right) + \frac{1}{(b q_m)} \quad (3.12)$$

where q_m and b are Langmuir constants related to the sorption capacity and sorption energy, respectively, C_e is the equilibrium concentration in mg L^{-1} , and q_e is the amount of adsorbate adsorbed per unit weight of adsorbent mg g^{-1} . R_L in Table 3.11 is a dimensionless separation factor which indicates the favourability and the capacity of the adsorption system, and it is obtained from Equation 3.13 [35-42].

$$R_L = \frac{1}{1 + b C_o} \quad (3.13)$$

The R_L value indicates the adsorption nature to be either unfavourable ($R_L > 1$), linear ($R_L = 1$), favourable ($0 < R_L < 1$) or irreversible ($R_L = 0$).

The plot of C_e/q_e against C_e is shown in Figure 3.15. The adsorption of lead Pb(II) ions on the different adsorbents gives a straight line. It is clear that the linear fit is fairly good and enables the applicability of the Langmuir model. The Langmuir isotherm constants and their correlation coefficients R^2 are listed in Table 3.11. As can be observed, experimental data were better fitted to the Langmuir equation than to the Freundlich equation. The sorption process of metal ions on composites follows the Langmuir isotherm model, where the metal ions are taken up independently on a single type of binding site in such a way that the uptake of the first metal ion does not affect the sorption of the next ion. For the two studied systems, the Langmuir isotherm shows more significant correlation ($R^2 > 0.99$) than in the case of Freundlich isotherm.

The sorption capacity q_m is high for neat SCB and decreases for the composites, which is to be expected because the neat SCB was completely exposed to the metal ion solution. It was expected that the sorption capacity of the composites containing 30% of SCB will be higher

than that of the composites containing 15% of SCB, but the opposite was observed (Table 3.11). The sorption energy b was used to calculate the dimensionless separation factor R_L . The separation factor R_L indicates that the adsorption nature is favourable for the pure SCB as well as the composites since for all the samples $0 < R_L < 1$. The pure SCB shows a significantly higher value than the composites, which means that the pure SCB more effectively adsorbs the metal ions, which is according to expectation.

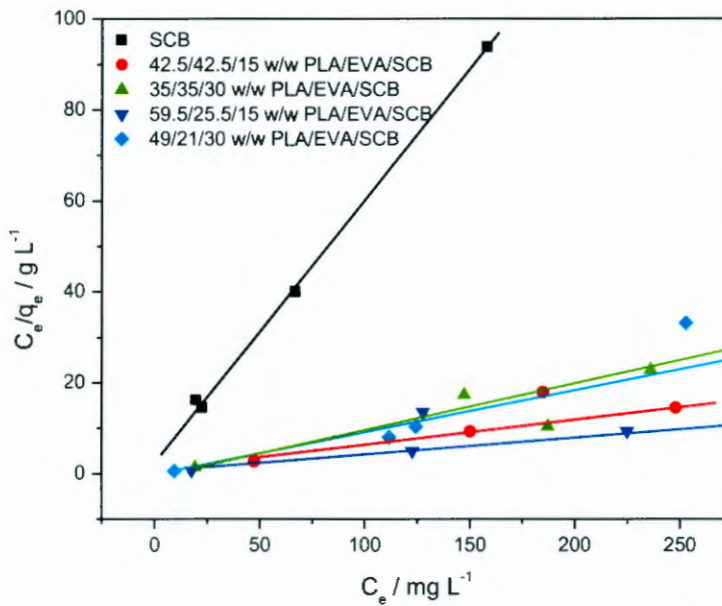


Figure 3.15 Langmuir plots from which the data in Table 3.7 were obtained

Table 3.11 Langmuir isotherm constants for the sorption of lead Pb(II) ions by different composite samples

Sample (w/w PLA/EVA/SCB)	Langmuir constants			R^2
	q_m	b	R_L	
0/0/100	29.4	0.0114	0.4673	0.9982
42.5/42.5/15	16.7	2.8113	0.0035	0.9984
35/35/30	10.6	0.0964	0.0940	0.9823
59.5/25.5/15	22.8	0.1491	0.0629	0.9983
49/21/30	8.6	0.1080	0.0847	0.9553

3.7 References

- [1] S. Rimdusit, W. Tanthapanichakoon, C. Jubsilp. High Performance Wood Composites from Highly Filled Polybenzoxazine. *Journal of Applied Polymer Science* 2006; 99:1240–1253.
DOI: 10.1002/app.22607
- [2] J.P. Mofokeng, A.S. Luyt. Morphology and thermal degradation studies of melt-mixed PLA/PHBV biodegradable polymer blend nanocomposites with TiO₂ as filler. *Journal of Applied Polymer Science* 2015; 132:1-11.
DOI: 10.1002/app.42138
- [3] D. Pasquini, M.N. Belgacem, A. Gandini, A.A.S. Curvelo. Surface esterification of cellulose fibers: Characterization by DRIFT and contact angle measurements. *Journal of Colloid and Interface Science* 2006; 295:79-83.
DOI: 10.1016/j.jcis.2005.07.074
- [4] D. Wu, D. Lin, J. Zhang, W. Zhou, M. Zhang, Y. Zhang, D. Wang, B. Lin. Selective localization of nanofillers: Effect on morphology and crystallization of PLA/PCL blends. *Macromolecular Chemistry and Physics* 2011; 212:613-626.
DOI: 10.1002/macp.201000579
- [5] X. Wang, K. Xu, X. Xu, S. Park, S. Kim. Selective particle distribution and mechanical properties of nano-CaCO₃/ethylene-propylene-diene terpolymer/ polypropylene composites with high content of nano-CaCO₃. *Journal of Applied Polymer Science* 2009; 113: 2485-2491.
DOI: 10.1002/app
- [6] H. Xiu, H.W. Bai, C.M. Huang, C.L. Xu, X.Y. Li, Q. Fu. Selective localization of titanium dioxide nanoparticles at the interface and its effect on the impact toughness of poly(L-lactide)/poly(ether)urethane blends. *Express Polymer Letters* 2013; 7:261-271.
DOI: 10.3144/expresspolymlett.2013.24
- [7] F. Fenouillot, P. Cassagnau, J.C. Majesté. Uneven distribution of nanoparticles in immiscible fluids: Morphology development in polymer blends. *Polymer* 2009; 50:1333-1350.
DOI: 10.1016/j.polymer.2008.12.092
- [8] B. Zhao, R.W. Fu, M.Q. Zhang, H. Yang, M.Z. Rong, Q. Zheng. Effect of soft segments of waterborne polyurethane on organic vapour sensitivity of carbon black filled waterborne polyurethane composites. *Polymer Journal* 2006; 38:799-806.
DOI: 10.1295/polmj.PJ2005202

- [9] J.I. Morán, V.A. Alvarez, V.P. Cyras, A. Vázquez. Extraction of cellulose and preparation of nano-cellulose from sisal fibers. *Cellulose* 2008; 15:149-159.
DOI: 10.1007/s10570-007-9145-9
- [10] X.F. Sun, R.C. Sun, Y. Su, J.X. Sun. Comparative study of crude and purified cellulose from wheat straw. *Journal of Agricultural and Food Chemistry* 2004; 52:839-847.
DOI: 10.1021/jf0349230
- [11] H. Yang, R. Yang, H. Chen, D.H. Lee, C. Zheng. Characteristics of hemicellulose, cellulose and lignin pyrolysis. *Fuel* 2007; 86:1781-1788.
DOI: 10.1016/j.fuel.2006.12.013
- [12] R. Maryana, D. Ma'rifatun, A.I. Wheni, K.W. Satriyo, W.A. Rizal. Alkaline pretreatment on sugarcane bagasse for bioethanol production. *Energy Procedia* 2014; 47:250-254.
DOI: 10.1016/j.egypro.2014.01.221
- [13] A. Kumar, Y.S. Negi, V. Choudhary, N.K. Bhardwaj. Characterization of cellulose nanocrystals produced by acid-hydrolysis from sugarcane bagasse as agro-waste. *Journal of Materials Physics and Chemistry* 2014; 2:1-8.
DOI:10.12691/jmpc-2-1-1
- [14] M.K. Hossain, M.R. Karim, M.R. Chowdhury, M.A. Imam, M. Hosur, S. Jeelani, R. Farag. Comparative mechanical and thermal study of chemically treated and untreated single sugarcane fiber bundle. *Industrial Crops and Products* 2014; 58:78-90.
DOI: 10.1016/j.indcrop.2014.04.002
- [15] S. Chen, J. Zhang, J. Su. Effect of damp-heat aging on the properties of ethylene vinylacetate copolymer and ethylene acrylic acid copolymer blends. *Journal of Applied Polymer Science* 2009; 114:3110-3117.
DOI: 10.1002/app.30859
- [16] V. Krikorian, D.J. Pochan. Crystallization behaviour of poly(L-lactic acid) nanocomposites: Nucleation and growth probed by infrared spectroscopy. *Macromolecules* 2005; 38:6520-6527.
DOI: 10.1021/ma050739z
- [17] P. Penjumras, R.A. Rahman, R.A. Talib, K. Abdan. Response surface methodology for the optimization of preparation of biocomposites based on poly(lactic acid) and durian peel cellulose. *The Scientific World Journal* 2015; 2015:1-12.
DOI:10.1155/2015/293609

- [18] A. Lazzeri, S.M. Zebarjad, M. Pracella, K. Cavalier, R. Rosa. Filler toughening of plastics. Part 1 - The effect of surface interactions on physico-mechanical properties and rheological behaviour of ultrafine CaCO₃/HDPE nanocomposites. *Polymer* 2004; 46:827-844.
DOI: 10.1016/j.polymer.2004.11.111
- [19] D.N. Saheb, J.P. Jog. Natural fibre polymer composites: A review. *Advances in Polymer Technology* 1999; 18:351-363.
DOI: 10.1002/(SICI)1098-2329(199924)18:4<351:AID-ADV6>3.0.CO;2-X
- [20] K.L. Pickering, M.G.A. Efendy, T.M. Le. A review of recent developments in natural fibre composites and their mechanical performance. *Composites Part A* 2015 (published online).
DOI: 10.1016/j.compositesa.2015.08.038
- [21] U.S. Bongarde, V.D. Shinde. Review on natural fiber reinforcement polymer composites. *International Journal of Engineering Science and Innovative Technology (IJESIT)* 2014; 3:431-436.
- [22] N. Hatta, N. Akmar. Mechanical properties of polystyrene/polypropylene reinforced coconut and jute fibres. *CUTSE International Conference 2008, 24-27 November 2008, Miri, Sarawak, Malaysia.*
- [23] B. Rimez, H. Rahier, G. Van-Assche, T. Artoos, M. Biesemans, B. Van-Mele. Thermal degradation of poly(vinyl acetate) and poly(ethylene-co-vinyl acetate), Part I: Experimental study of the degradation mechanism. *Polymer Degradation and Stability* 2008; 93:800-810.
DOI: 10.1016/j.polymdegradstab.2008.01.010
- [24] R.C.L. Dutra, B.G. Soares. Determination of the vinyl mercaptoacetate content in poly(ethylene-co-vinyl acetate-co-vinyl mercaptoacetate) (EVASH) by TGA analysis and FTIR spectroscopy. *Polymer Bulletin* 1998; 41:61-67.
DOI: 10.1007/s002890050333
- [25] M.K. Hossain, M.R. Karim, M.R. Chowdhury, M.A. Imam, M. Hosur, S. Jeelani, R. Farag. Comparative mechanical and thermal study of chemically treated and untreated single sugarcane fiber bundle. *Industrial Crops and Products* 2014; 58:78-90.
DOI: 10.1016/j.indcrop.2014.04.002

- [26] C.G. Mothé, I.C. de Miranda. Study of kinetic parameters of thermal decomposition of bagasse and sugarcane straw using Friedman and Ozawa–Flynn–Wall isoconversional methods. *Journal of Thermal Analysis and Calorimetry* 2013; 113:497-505.
DOI: 10.1007/s10973-013-3163-7
- [27] H. Yang, R. Yan, H. Chen, D.H. Lee, C. Zheng. Characteristics of hemicellulose, cellulose and lignin pyrolysis. *Fuel* 2007; 86:1781-1788.
DOI: 10.1016/j.fuel.2006.12.013
- [28] T.E. Motaung, R.D. Anandjiwala. Effect of alkali and acid treatment on thermal degradation of kinetics of sugarcane bagasse. *Industrial Crops and Products* 2015; 74:472-477.
DOI: 10.1016/j.incrop.2015.05.062
- [29] B. Rimez, H. Rahier, G. Van Assche, T. Artoos, M. Biesemans, B. Van Mele. The thermal degradation of poly(vinyl acetate) and poly(ethylene-co-vinyl acetate), Part I: Experimental study of the degradation mechanism. *Polymer Degradation and Stability* 2008; 93:800-810.
DOI: 10.1016/j.polymdegradstab.2008.01.010
- [30] A. Espert, F. Vilaplana, S. Karlsson. Comparison of water absorption in natural cellulosic fibres from wood and one-year crops in polypropylene composites and its influence on their mechanical properties. *Composites: Part A* 2004; 35:1267-1276.
DOI:10.1016/j.compositesa.2004.04.004
- [31] H.N. Dhakal, Z.Y. Zhang, M.O.W. Richardson. Effect of water absorption on the mechanical properties of hemp fibre reinforced unsaturated polyester composites. *Composites Science and Technology* 2007; 67:1674-1683.
DOI:10.1016/j.compscitech.2006.06.019
- [32] S.K. Najafi, M. Tajvidi, M. Chaharmahli. Long-term water uptake behavior of lignocellulosic-high density polyethylene composites. *Journal of Applied Polymer Science* 2006; 102:3907-3911.
DOI: 10.1002/app.24172
- [33] H.S. Yang, H.J. Kim, H.J. Park, B.J. Lee, T.S. Hwang. Water absorption behavior and mechanical properties of lignocellulosic filler–polyolefin bio-composites. *Composite Structures* 2006; 72:429-437.
DOI:10.1016/j.compstruct.2005.01.013
- [34] A. Arbelaiz, B. Fernández, J.A. Ramos, A. Retegi, R. Llano-Ponte, I. Mondragon. Mechanical properties of short flax fibre bundle/polypropylene composites: Influence

- of matrix/fibre modification, fibre content, water uptake and recycling. *Composites Science and Technology* 2005; 65:1582-1592.
DOI: 10.1016/j.compscitech.2005.01.008
- [35] O.E.A. Salam, N.A. Reiad, M.M. ElSha. A study of the removal characteristics of heavy metals from wastewater by low-cost adsorbents. *Journal of Advanced Research* 2011; 2:297-303.
DOI: 10.1016/j.jare.2011.01.008
- [36] S. Lin, Z. Song, G. Che, A. Ren, P. Li, C. Liu, J. Zhang. Adsorption behavior of metal-organic frameworks for methylene blue from aqueous solution. *Microporous and Mesoporous Materials* 2014; 193:27-34.
DOI: 10.1016/j.micromeso.2014.03.004
- [37] K.Y. Foo, B.H. Hameed. Insights into the modeling of adsorption isotherm systems. *Chemical Engineering Journal* 2010;156:2-10.
DOI: 10.1016/j.cej.2009.09.013
- [38] M. Monier, D.A. Abdel-Latif. Modification and characterization of PET fibers for fast removal of Hg(II), Cu(II) and Co(II) metal ions from aqueous solutions. *Journal of Hazardous Materials* 2013;250-251:122-130.
DOI: 10.1016/j.jhazmat.2013.01.056
- [39] H. Surikumaran, S. Mohamad, N.M. Sarih. Molecular imprinted polymer of methacrylic acid functionalised β -cyclodextrin for selective removal of 2,4-dichlorophenol. *International Journal of Molecular Sciences* 2014; 15:6111-6136.
DOI: 10.3390/ijms15046111
- [40] M. Li, M.-y. Li, C.-g. Feng, Q.-x. Zeng. Preparation and characterization of multi-carboxyl-functionalized silica gel for removal of Cu (II), Cd (II), Ni (II) and Zn (II) from aqueous solution. *Applied Surface Science* 2014; 314:1063-1069.
DOI: 10.1016/j.apsusc.2014.06.038
- [41] S.C. Ibrahim, M.A.K.M. Hanafiah, M.Z.A. Yahya. Removal of cadmium from aqueous solutions by adsorption onto sugarcane bagasse. *American-Eurasian Journal of Agriculture and Environmental Science* 2006; 1:179-184.
- [42] U. Garg, M.P. Kaur, G.K. Jawa, D. Sud, V.K. Garg. Removal of cadmium (II) from aqueous solutions by adsorption on agricultural waste biomass. *Journal of Hazardous Materials* 2008; 154:1149-1157.
DOI: 10.1016/j.jhazmat.2007.11.040

CHAPTER 4

Conclusions

The purpose of this project was to prepare polymer/natural fibre composites to be used in water purification applications, specifically to remove lead ions from contaminated water. PLA/EVA blends (as control samples) and PLA/EVA/SCB composites were successfully prepared by melt mixing. The results show that SCB had a stronger affinity for PLA than for EVA. PLA and EVA were also completely immiscible, with the 50/50 w/w PLA/EVA sample showing a co-continuous morphology and the 70/30 w/w PLA/EVA sample showing EVA dispersed as small spheres in the continuous PLA phase. Good wetting of the SCB fibre by the PLA was observed in the composites, but exposed fibre ends were observed in some SEM pictures which would add to the efficiency of metal adsorption.

The two polymers in the blend seemed to have protected the SCB from thermal degradation, because the mass loss of SCB degradation products was only observed at higher temperatures when incorporated in the blends. Although this behaviour may imply that the prepared composites can be used at temperatures above 200 °C, which is the degradation temperature of pure SCB, it is also possible that the release of the volatile SCB degradation products was delayed as a result of interaction with one or both polymers. The impact properties depended more on the PLA:EVA ratio than on the presence of SCB.

The main aim of this research was to formulate effective and environmentally friendly biocomposites for the removal of lead from contaminated water. The goal was successfully achieved, since all the investigated samples adsorbed the lead. It was observed that more lead was adsorbed than one would expect if the partial coverage of the fibre by polymer is taken into account, and therefore it may be assumed that some of the lead was trapped inside the cavities in the composites and that the polymers may also have played a role in the metal complexation process, since both polymers have the functional groups that could interact with the lead ions. It was found that monolayer adsorption was predominant, since the data best fitted the Langmuir adsorption isotherm.

In conclusion, the 50/50/15 w/w PLA/EVA/SCB sample gave the best adsorption values, because this sample has a more co-continuous morphology that provides continuous pathways between the two incompatible polymers that allowed more effective penetration of the solution into the composite. While it was found that the 70/30 w/w PLA/EVA based samples have better impact strengths than the 50/50 w/w PLA/EVA based samples, the differences are not significant and therefore the 50/50/15 w/w PLA/EVA/SCB composite has an acceptable balance of properties to be used for the purpose of water purification.

Recommendation or future work:

- Use of the blowing agent in the composites to form a porous membrane that will help the metal impurities to more easily come into contact with the fibre.
- Do a desorption study to check if the composites can be reused after the removal of metal impurities from water.

ACKNOWLEDGEMENTS

First of all I would like to thank God who gave me strength, blessing, and courage during this study and during all of my life.

I would like to express my deepest and profound gratitude to my supervisors **Prof. Adriaan Stephanus Luyt and Mr. Khotso Mpitso** for their guidance, encouragement, and endless support during my masters study. I learned a lot throughout their supervision. I really feel that words will not express my appreciation to whatever they have done for me.

During my time in postgraduate level, our group has seen many different faces. I am lucky to have interacted with so many people with vastly different backgrounds. Some people directly helped with my research, while others simply set a good example of hard work and fortitude. My genuine gratitude goes to all the colleagues in the Polymer Research Group of UFS (Qwaqwa campus), Ms. Thandi Gumede, Ms. Cheryl-Ann Clarke, Ms. Motshabi Sibeko, Dr. Puseletso Mofokeng, Mr. Tsietsi Tsotetsi, Mr. Tyson Mosoabisane, Dr. Shale Sefadi, Mr. Benison Motloun, Mrs. Mothezana Radebe, Mrs. Moipone Malimabe, Dr. Nomampondomise Molefe, Mr. Rantoa Moji, Mrs. Marlize Jackson, Dr. Duško Dudić and Dr. Lebohang Hlalele. Special thanks to Mr. Mfiso Mngomezulu for the fruitful discussions we had on my project and for always willing to help me.

I acknowledge Mr. Patrick Komane from the University of Johannesburg for AAS analysis of my samples, and Dr Tshwafo Motaung from the University of Zululand for providing me with SCB, I really appreciate the good work you did.

The support I have received from my family is immeasurable. They have been supportive of all aspects of my life, especially education. I cannot thank them enough.

Special thanks to Mr. Edwin Lecheko for the constant support, encouragement and patience throughout my studies.

Lastly, I am very grateful for the financial support I received from the National Research Foundation (NRF) and Sasol Inzalo Foundation (SaIF), South Africa.

Appendix

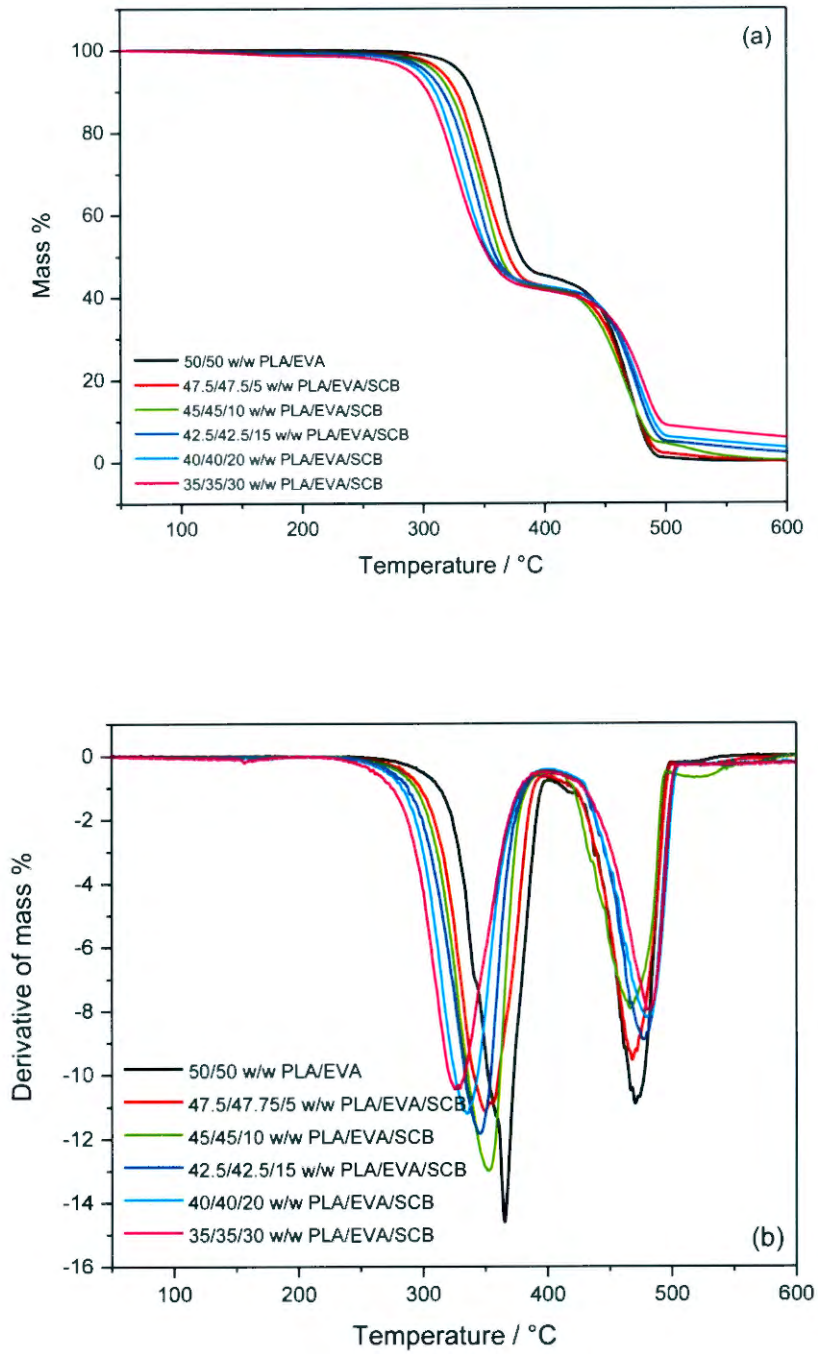


Figure A.5 (a) TGA and (b) derivative TGA curves of 50/50 w/w PLA/EVA and its bio-composites

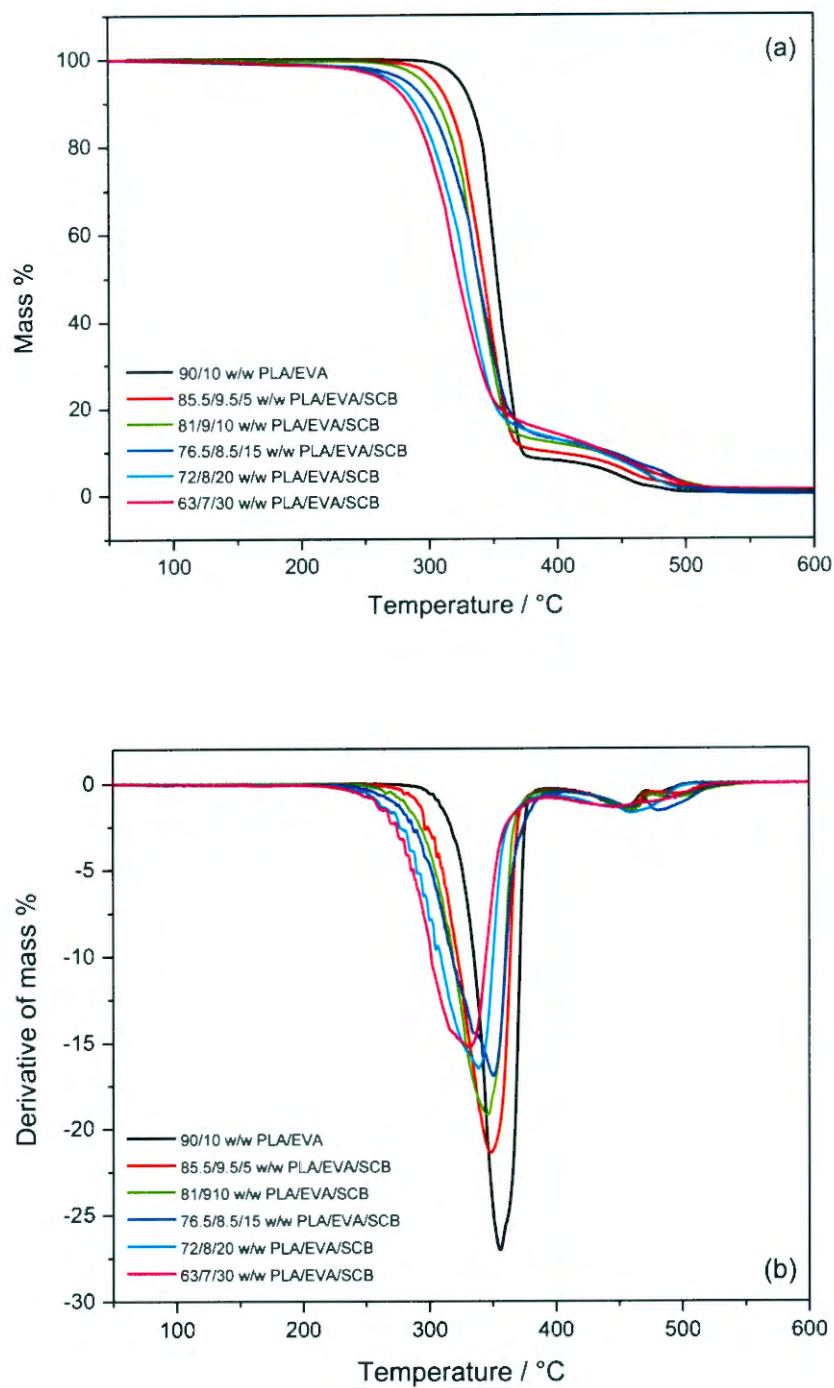


Figure A.6 (a) TGA and (b) derivative TGA curves of 90/10 w/w PLA/EVA and its bio-composites

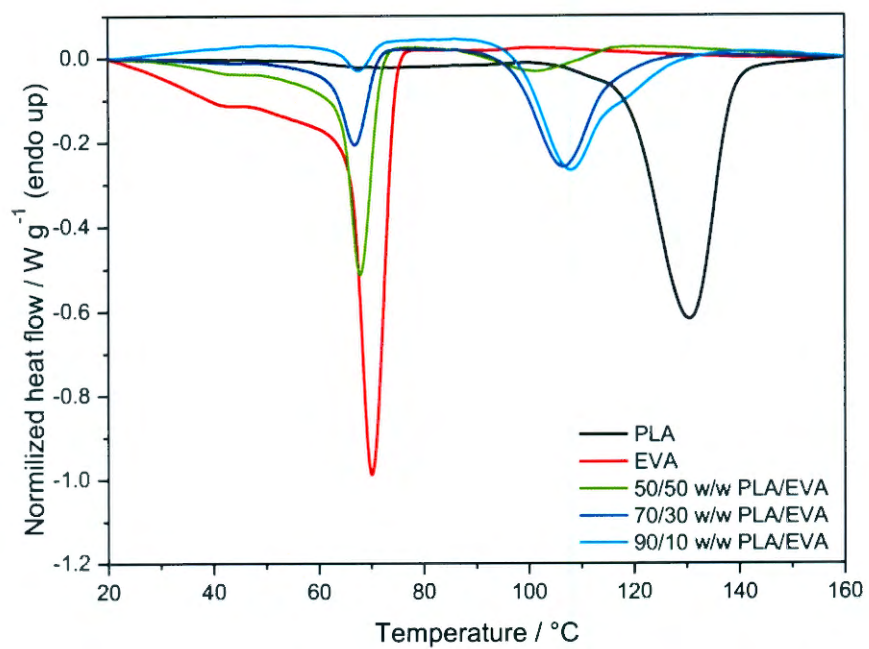


Figure B.1 DSC cooling curves of the neat PLA, EVA and the PLA/EVA blends